Site-Selective Benzannulation of *N*-Heterocycles in Bidentate Ligands Leads to Blue-Shifted Emission from $(P\text{^}N)_2Cu_2X_2$ Dimers

Rajarshi Mondal,[a] Issiah B. Lozada,[a] Rebecca L. Davis,[a] J. A. Gareth Williams[b] and David E. Herbert[a*]*

[a]Department of Chemistry and the Manitoba Institute for Materials, University of Manitoba, 144 Dysart Road, Winnipeg, Manitoba, R3T 2N2, Canada.

*david.herbert@umanitoba.ca

[b]Department of Chemistry, Durham University, Durham, DH1 3LE, U.K.

*j.a.g.williams@durham.ac.uk

ABSTRACT

Benzannulated bidentate pyridine/phosphine (P^N) ligands bearing quinoline or phenanthridine (3,4-benzoquinoline) units have been prepared, along with their halide-bridged dimeric Cu(I) complexes of the form $[(P\text{^}N)Cu]_2(\mu\text{-}X)_2$. The copper complexes are phosphorescent in the orange-red region of the spectrum in the solid state under ambient conditions. Structural characterization in solution and the solid-state reveals a flexible conformational landscape, with both diamond-like and butterfly motifs available to the Cu_2X_2 cores. Comparing the photophysical properties of complexes of (quinolinyl)phosphine ligands with those of π-extended (phenanthridinyl)phosphines has revealed a counter-intuitive impact of site-selective benzannulation. Contrary to conventional assumptions regarding π-extension and a bathochromic shift in the lowest energy absorption maxima, a blue shift of nearly 40 nm in the emission wavelength is observed for the complexes with larger ligand π-systems, which is assigned as phosphorescence on the basis of emission energies and lifetimes. Comparison of the ground-state and triplet excited state structures optimized from TD-DFT calculations allows attribution of this effect to a greater rigidity for the benzannulated complexes resulting in a higher energy emissive triplet state, rather than significant changes to orbital energies. This study reveals that ligand structure can impact photophysical properties for emissive molecules by influencing their structural rigidity, in addition to their electronic structure.

INTRODUCTION

Extending π-conjugation in a ligand system is a common strategy for adjusting photophysical properties in coordination complexes without significantly altering the parent ligand structure. This strategy introduces flexibility into the design of photosensitizers and emissive molecules, as properties can be tuned without substantial changes to the core coordination environment. Expanding conjugation typically induces bathochromic shifts of absorption and emission bands, as the frontier orbitals become progressively closer in energy with π-extension.[1-4] Recently, experimental systems[5-6] have begun to challenge the extent to which this conventional view is applicable and a theoretical framework[7] based on analysis of the site-dependent impact of π-extension on frontier molecular orbital energies has been developed. In this paradigm, the consequence of benzannulation is interpreted through the effect on HOMO/LUMO energies and the corresponding changes to the lowest lying singlet (S_1) and triplet (T_1) excited states.[6-7]

Curious as to the general applicability of this theoretical paradigm, we have developed synthetic routes to 2,4-disubstituted phenanthridines (phenanthridine = 3,4-benzoquinoline) that enable incorporation of this benzannulated aromatic *N*-heterocycle into multidentate ligand frameworks.[8-9] Surprisingly, within a series of pincer-type tridentate ligands, sequential quinoline-to-phenanthridine π-extension (e.g., from bis(8-quinolinyl)amido through (4-methylphenanthridinyl)(8-quinolinyl)amido to *bis*(4-methylphenanthridinyl)amido ligand frameworks) was found to *not* significantly affect the energy of absorption of the corresponding Ni^{2+}, Pd^{2+} and Pt^{2+} complexes: the complexes showed isoenergetic λ_{max} values,[9] despite benzannulation leading to changes

in the energies of the frontier orbitals, in line with the aforementioned theoretical models.[7] In that series of complexes, while stabilization of the lowest unoccupied molecular orbital (LUMO) was observed with π-extension, this was accompanied by a change in oscillator strength of the HOMO→LUMO and HOMO→LUMO+1 transitions, effectively shutting off the lower energy HOMO→LUMO transition in favor of the HOMO→LUMO+1. This resulted in near-identical UV-Vis absorption profiles despite the significant expansion of ligand conjugation.

In this work, we have prepared a series of luminescent halide-bridged, dimeric Cu(I) complexes of phenanthridine-containing, *P^N*-coordinating ligands (Figure 1; **1-X**, **2-X**: X = Cl, Br, I) and compared their photophysical properties with those of quinoline analogs (**3-X**: X = Cl, Br, I) comprising smaller π-systems. Cu(I) complexes are attracting increasing attention as low-cost luminescent materials, with applications in light-emitting devices, as photosensitizers, dyes and imaging agents.[10-14] Although the spin-orbit coupling (SOC) constant of copper is lower than that of 2nd and 3rd row elements like ruthenium, iridium and platinum, Cu(I) can nevertheless promote the formally forbidden phosphorescence from triplet states in some systems with π-acceptor ligands, owing to the efficiency of SOC pathways through coupling of the lowest triplet state with close-lying ^{1}MLCT states.[15] In some cases, meanwhile, a small S_1–T_1 energy gap can open up thermally activated delayed fluorescence (TADF) from T_1 to S_1 as another mechanism by which otherwise non-emissive triplet states can be harvested.[16] While the use of site-selective benzannulation in tuning emission has been reported for Pt[5, 7] and Ir[6] emitters, such strategies have not, to our knowledge, been explored in Cu(I)

coordination complexes. Whilst the results reveal more pronounced lower energy absorption bands upon extending the π-system, a counter-intuitive blue shift in emission maximum is observed. This contrary behavior was not observed for Pt[5, 7] or Ir,[6] where the direction of the shift was the same for both absorption and emission. A strong dependence of the luminescence efficiency on the identity of the halide bridge has also been discovered.

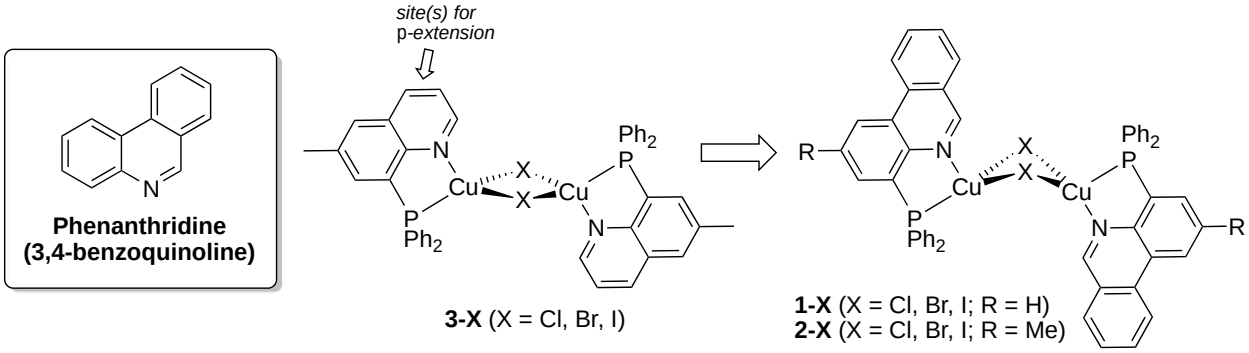

Figure 1. Site-selective benzannulation of quinoline ligand frameworks in $(P\text{^}N)_2Cu_2X_2$ complexes.

RESULTS AND DISCUSSION

Synthesis

Hybrid P^N donor proligands **L1** and **L2** were prepared from 4-bromophenanthridines as outlined in Scheme 1. The synthesis of **L1** and the dimeric Cu_2Br_2 compound **1-Br** has been previously disclosed.[8] We have since found that incorporating a methyl substituent in the 2-position allows higher yields of the 4-bromophenanthridine to be obtained compared with the unsubstituted analog (R = H),[9]

thereby increasing the overall yields of **L2** compared with **L1**. Following lithium-halogen exchange with *sec*-BuLi and quenching with Ph_2PCl as an electrophilic source of phosphorus, 4-(diphenylphosphino)-2-methylphenanthridine (**L2**) was isolated in 63% yield. The corresponding 6-methylquinoline analog incorporating a less extended π-system (**L3**) could similarly be isolated in 67% yield by starting from 8-bromo-6-methylquinoline.

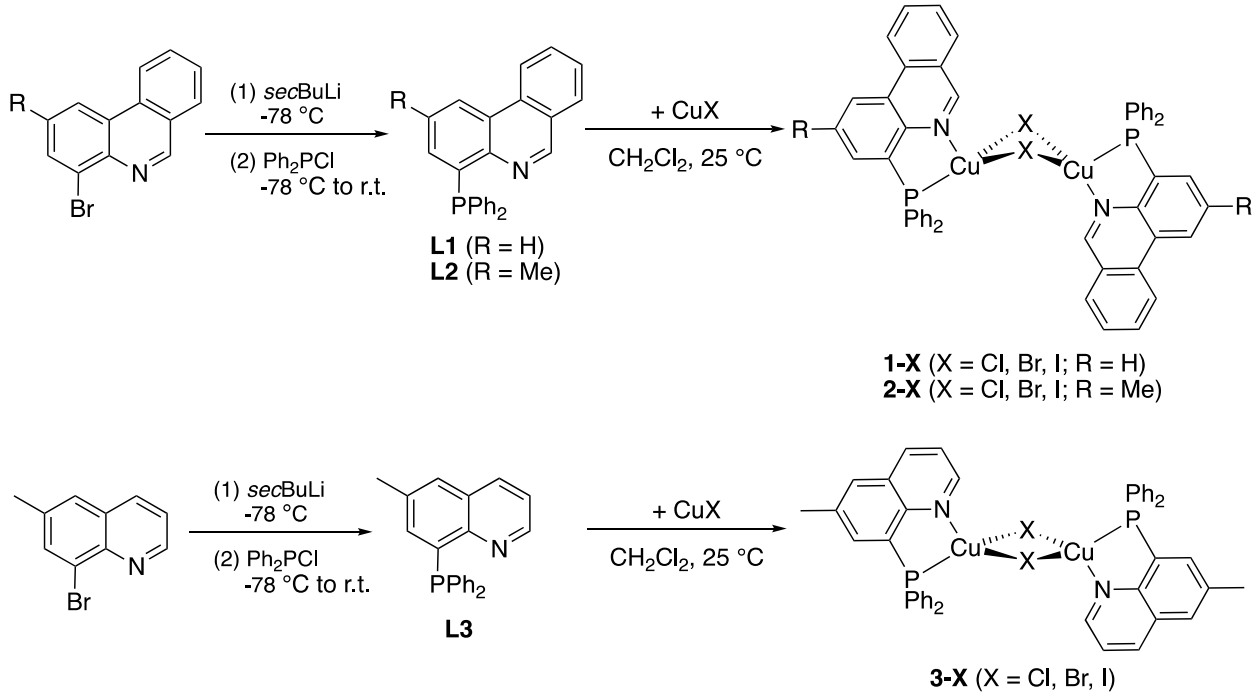

Scheme 1. Synthesis of π-extended phenanthridine-based *P^N*-coordinating proligands **L1** and **L2**, the parent quinoline-based analog **L3**, and the corresponding halide-bridged Cu_2X_2 dimers **1-X**, **2-X** and **3-X** (X = Cl, Br, I).

The structure of the phenanthridine subunit in **L1** and **L2** is best described as an 'imine-bridged biphenyl' in accordance with Clar's postulate, wherein the dominant resonance contributor maximizes the number of aromatic sextets in the polycyclic

aromatic system.[17] In the ^{1}H NMR spectra, the 'imine-like' hydrogen in the 6-position of the phenanthridine ring is thus observed at a chemical shift unusually downfield for an aromatic *N*-heterocycle [δ(C_6-*H*) **L2**: 9.19 ppm and **L1**: 9.23 ppm], as is the 'imine-like' carbon in the ^{13}C{^{1}H} NMR spectra [δ(*C_6*-H) **L2**: 151.8 ppm and **L1**: 152.8 ppm]. In the quinoline-containing **L3**, the comparable C-H unit *ortho* to N is less deshielded [δ(*C-H*) 8.79 (m) and 149.0 ppm in the ^{1}H and ^{13}C{^{1}H} spectra respectively]. For each proligand, one sharp singlet is observed in the ^{31}P{^{1}H} NMR spectra (–13.7 ppm for **L1**, –13.6 ppm for **L2** and –14.9 ppm for **L3**).

Addition of solutions of **L1**–**L3** in CH_2Cl_2 to suspensions of the appropriate CuX precursor (X = Cl, Br or I) led to the formation of yellow-orange solutions, which became increasingly homogeneous with conversion to the metallated products. Complexes **1-X**, **2-X** and **3-X** were isolated following recrystallization. They were fully characterized in solution by multi-nuclear NMR spectroscopy and in the solid-state by elemental analysis and, for **2-X** and **3-X**, single-crystal X-ray diffraction. Quantitative yields of **1-X**, **2-X** and **3-X** were also obtained via simple solid-phase grinding[18] of the appropriate ligand (**L1-3**) with CuX, with identical solution NMR parameters observed for products from solution or solid-state synthesis (see Figures S1-S7).

In the solid-state, most of the complexes adopt a 'diamond core'-like Cu_2X_2 motif, in which all four of the central atoms – the two copper ions and the two halides – are mutually coplanar (Figure 2a,b and Figure 3). In contrast, **2-I** and **1-Br**[8] adopt 'butterfly'-type structures, in which the two halides bend out of the plane towards one of the *P^N* ligands. In this structural motif, the molecule no longer bears a center of

symmetry, but has two edge-sharing Cu–X–Cu triangles closer to one *P^N* ligand than the other (Figure 2c). Both butterfly-type structures include a co-crystallized CH_2Cl_2 molecule in the lattice. In solution, only one set of ligand signals is evident by ^1H and $^{13}C\{^1H\}$ NMR spectroscopy for all compounds, suggesting fluxional structures that render the ligand environments equivalent on the NMR timescale, despite their inequivalence in the solid state in **2-I** and **1-Br**. In addition, for **2-Br** both types of structural motifs could be crystallized according to the crystallization conditions (Figure S8), with lattice-confined solvents favoring bent, butterfly-like structures, suggesting a soft energy landscape for the two geometries. A further possible isomer is a 'head-to-head' orientation of the two *P^N* ligands, where both phosphines are positioned on the same side of the Cu_2X_2 core. This seems unlikely to be relevant on steric grounds, as the two sets of phenyl rings of the PPh_2 units would clash much more significantly than the phenanthridine/PPh_2 combination in the 'head-to-tail' orientation observed in the solid-state.

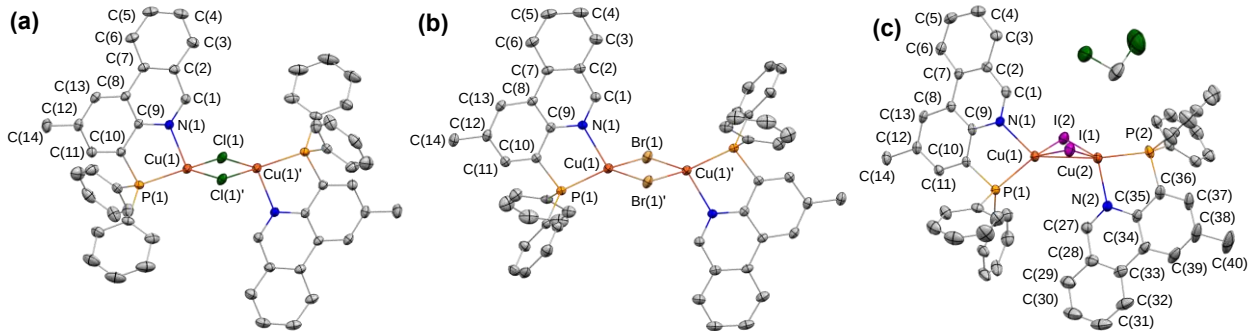

Figure 2. ORTEPs[19] of the solid-state structures of (a) **2-Cl**, (b) **2-Br** and (c) **2-I**. Ellipsoids are shown at 50% probability levels with hydrogen atoms, symmetry-generated and phenyl ring atom labels omitted for clarity in (a) and (b). In (c), an

additional CH_2Cl_2 solvent molecule (beyond the one depicted) was found in the lattice but omitted here for clarity.

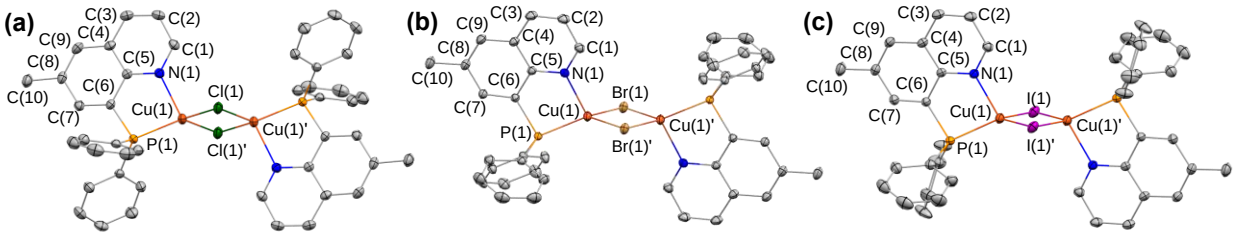

Figure 3. ORTEPs[19] of the solid-state structures of (a) **3-Cl**, (b) **3-Br** and (c) **3-I**. Ellipsoids are shown at 50% probability levels with hydrogen atoms, symmetry-generated and phenyl ring atom labels omitted for clarity.

Table 1. Selected bond lengths (Å) and angles (°) of Cu_2X_2 complexes

	2-Cl	**2-Br**	**2-I**[a]	**3-Cl**	**3-Br**	**3-I**
Cu(1)-P(1)	2.1772(5)	2.2122(6)	2.2291(9), 2.2369(9)[b]	2.1934(6)	2.2088(3)	2.2365(4)
Cu(1)-N(1)	2.0969(11)	2.1386(16)	2.100(3), 2.102(3) [b]	2.1287(16)	2.1161(9)	2.1077(12)
Cu(1)-X(1)	2.3035(5)	2.4775(3)	2.5710(5)	2.3613(6)	2.4697(2)	2.6071(2)
Cu(1)-X(1)'	2.3795(7)	2.4862(3)	2.6854(5)[b]	2.3450(5)	2.47492(19)	2.6259(3)
Cu(1)-Cu(1)'	2.9990(7)	3.3246(5)	2.7082(6)	2.9802(5)	3.0077(3)	2.7227(4)
N(1)-Cu(1)-P(1)	86.09(3)	84.73(5)	84.77(8), 85.17(8)[b]	85.90(5)	86.28(2)	85.96(3)
X(1)-Cu(1)-X(1)'	100.376(18)	95.900(11)	111.995(16), 112.273(18)[b]	101.421(18)	105.068(6)	117.299(7)

[a] Structure has 'butterfly' Cu_2I_2 core and is a solvate with two molecules of CH_2Cl_2 located in the lattice.

[b] Cu(2)–P(2), Cu(2)–N(2), Cu(2)–I(2) lengths; N(2)-Cu(2)-P(2) and I(1)-Cu(2)-I(2) angles.

Within each series of complexes, the Cu–X distances increase as expected with increasing ionic radius of the halide, as do the intramolecular Cu···Cu distances for the chloro- and bromo-containing 'diamond-core' structures; e.g., **2-Cl** [2.9990(7) Å] compared with **2-Br** [3.3246(5) Å] (Table 1). In the bent butterfly geometry of **2-I**, the two metals are able to approach each other more closely, leading to a significantly shorter Cu···Cu distance of 2.7082(6) Å. The Cu···Cu distance in **3-I** [2.7227(4) Å] is similarly

the shortest within the **3-X** series [**3-Cl**: 2.9802(5) Å; **3-Br** 3.0077(3) Å], even though a coplanar Cu_2X_2 arrangement is maintained in each case. In the structure of **3-I**, longer Cu-I bond distances [2.6071(2), 2.6259(3) Å; *cf.* ~ 2.3 (**3-Cl**), ~2.4 Å (**3-Br**)] enable a considerably wider I–Cu–I angle [117.299(7)° compared to 105.068(6)° and 101.421(2)° for **3-Br** and **3-Cl** respectively], allowing a closer approach of the two Cu centers. The Cu–P bond lengths increase with halide radius, whereas the Cu–N distances do not follow the same trend, decreasing with increasing halide radius within series **3-X**.

Interestingly, in the ^{1}H NMR spectra of the complexes in solution, the resonance assigned to the diagnostic proton in the 'imine-like' position of the phenanthridine-containing ligands is increasingly shifted downfield comparing the chloro to the bromo to the iodo member within each series **1-X**, **2-X** and **3-X**. In the solid-state structures, the intramolecular distance between this proton (C_6-H) and the halides of the Cu–X–Cu bridge decreases in the order of X = I > Br > Cl. The chloride in **1-Cl** can be interpreted, therefore, as exhibiting the closest hydrogen-halide bonding, which manifests in a more significant shielding of the diagnostic proton nucleus and an upfield shift in the ^{1}H NMR spectrum. In the ^{31}P{^{1}H} NMR spectra of **1-X**, the metal-bound phosphorus appears as a broad peak, shifted upfield from the proligand (**1-Cl**: -17.9, **1-Br**: -24.0, **1-I**: -28.3 ppm; **2-Cl**: -17.2, **2-Br**: -22.5, **2-I**: -27.8 ppm; and **3-Cl**: -18.2, **3-Br**: -23.7, **3-I**: -29.9 ppm), with the size of the upfield shift corresponding to the size of the halide [δ_P(Cl) > δ_P(Br) > δ_P(I)].

Electronic Absorption and Photoluminescence

UV-Vis absorption spectra were collected for all nine complexes in solution in CH_2Cl_2 at ambient temperature. As expected from their orange color, the complexes absorb strongly in the UV with a tail into the visible region (Figure 4). The spectra of the phenanthridine-containing compounds (**1-X** and **2-X**) contain additional low energy features compared with the quinoline derivatives (**3-X**), with a well-resolved maximum at 353 nm (**1-X**), slightly red-shifted for the methyl derivatives (**2-X**: λ_{max} = 355 nm**)**, and a peak/shoulder at 340 nm. In comparison, the quinoline-containing complexes all show lower molar absorptivities and absorption spectra shifted firmly into the UV and edge of the visible.

Comparison with the UV-visible spectra of the corresponding ligands is informative. Thus, **L1** and **L2** show bands around 350 and 335 nm (Figure S9) that resemble those in the spectra of the corresponding copper complexes. A series of bands in this region, albeit a little sharper, is in fact, characteristic of phenanthridine itself and typical also of many of its derivatives.[20] On the other hand, the quinoline ligand **L3** displays a blue-shifted absorption spectrum relative to its phenanthridine analogues, with a broad band centered at 323 nm. The lower energy of absorption of the phenanthridine compared to the quinoline ligands is consistent with the intuitive expectation that a more conjugated system will typically have lower energy transitions associated with it. The main difference between the spectra of the three ligands and their copper(I) complexes is the presence of the long-wavelength tail in the complexes. These tails can reasonably be attributed to relatively weak, spin-allowed charge-transfer transitions (^{1}CT), in which the acceptor in the CT process is the heterocycle, based on assignments of Cu(I) complexes with related nitrogenous heterocyclic ligands. Whilst such transitions in homoleptic

$[Cu(N\text{^}N)_2]^+$ complexes have clear-cut ^{1}MLCT assignments (i.e., with the donor orbitals being of predominantly metal-based *d* character),[11] in the present heteroleptic complexes featuring relatively electron-rich halide ligands, the donor orbitals in the CT process would be more likely to comprise of molecular orbitals spanning both the metal and the halide; i.e., $^1\{d_{Cu}/p_X \rightarrow \pi^*_{N\text{^}P}\}$ or alternatively denoted ^{1}(M+X)LCT. Calculations using time-dependent density functional theory (TD-DFT) support this assignment (*vide infra*). Such conclusions have been deduced previously for related P^N ligand-supported Cu_2X_2 dimers bearing both diphenylphosphino and pyridinyl donors.[18, 21] In these related complexes, the lowest-energy transitions involve significant contributions from the frontier orbitals and are assigned as mainly HOMO-LUMO transitions, contributing significantly to the first excited singlet (S_1) and triplet (T_1) states of the complexes.[18, 21]

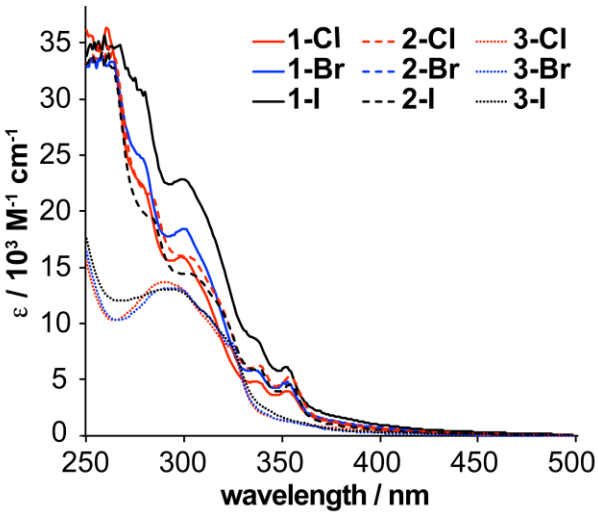

Figure 4. UV-Vis absorption spectra of **1-X**, **2-X** and **3-X** in CH_2Cl_2 solution at room temperature.

The three iodo complexes appear quite brightly luminescent to the eye when observed as powdered samples under long-wavelength UV irradiation, glowing orange/red (Figure S1). The bromo complexes are also visibly red luminescent, whilst for the chloro complexes, the emission is at best faint. The emission of the samples was studied in the solid state at ambient temperature using an integrating sphere to estimate photoluminescence quantum yields (Φ_{lum}) under continuous-wave excitation, whilst pulsed laser diode excitation was used to measure the luminescence lifetimes (τ) of the samples. The emission in dilute glassy solution at 77 K was also studied. At room temperature in solution, only very weak emission is observed, at similar wavelengths to the free ligand. This weak emission is therefore attributed to free ligand resulting from dissociation, in amounts barely perceptible by emission spectroscopy and unobservable by NMR spectroscopy. Representative spectra are shown in Figures 5–7 with data summarized in Table 2.

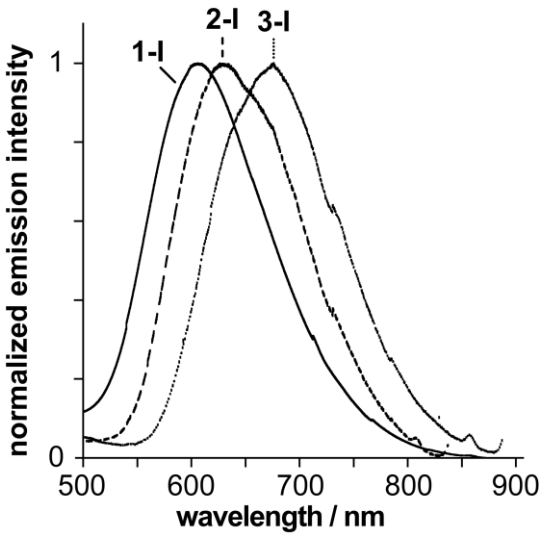

Figure 5. Emission spectra of **1-I**, **2-I** and **3-I** in the solid state at 298 ± 3 K, λ_{ex} = 425 nm.

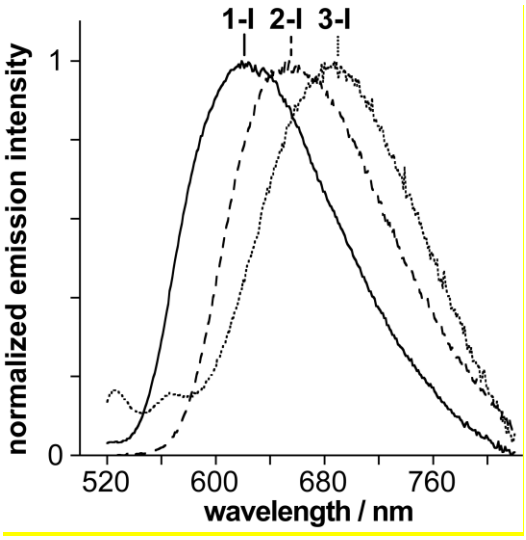

Figure 6. Emission spectra of **1-I**, **2-I** and **3-I** in EPA glass at 77 K, λ_{ex} = 425 nm. EPA = diethyl ether / isopentane / ethanol (2:2:1 v/v).

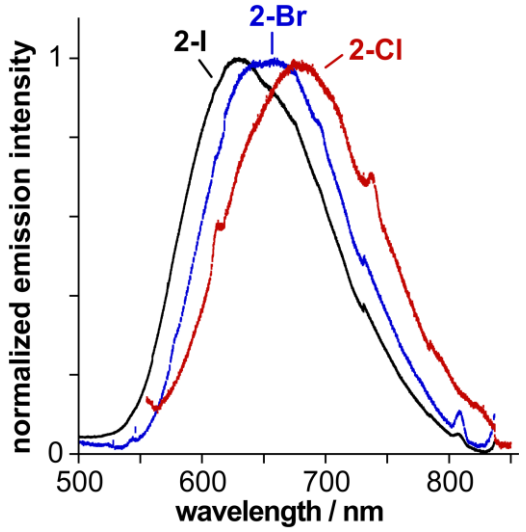

Figure 7. Emission spectra of **2-Cl**, **2-Br** and **2-I** in the solid state at 298 ± 3 K, λ_{ex} = 425 nm.

Table 2. Summary of photophysical data for **1-X**, **2-X** and **3-X**[a]

Compound	Emission[b] λ_{max} / nm	Φ_{lum} x 10^2	τ / ns [c]	k_r / 10^3 s^{-1} [d]	k_{nr} / 10^5 s^{-1} [d]	Emission 77 K[e]	
						λ_{max} / nm	τ / ns
1-Cl	682[f]	--[f]	150	--	--	[h]	[h]
1-Br	655	0.42	630	6.7	16	[h]	[h]
1-I	606	2.4	3200	7.5	3.1	622	81000
2-Cl	679	0.14	240	5.8	42	636	91000
2-Br	655	0.70	810	8.6	12	660	38000
2-I	630	1.2	1000	12.0	9.9	656	34000
3-Cl	--[g]	--[g]	--[g]	--	--	667	18000, 110000[i]
3-Br	691	0.05	250	2.0	40	690	15000
3-I	674	0.62	1000	6.2	9.9	687	18000

[a] Data are for solid state (powdered) samples except for 77 K data. [b] Room temperature, recorded using an integrating sphere and CCD detector; λ_{ex} = 425 nm. [c] λ_{ex} = 405 nm. [d] Radiative k_r and non-radiative Σk_{nr} rate constants as estimated from quantum yield and lifetime (see text). [e] In a glass of composition diethyl ether / isopentane / ethanol (2:2:1 v/v). [f] The intensity is weak and the spectrum of too poor quality to determine a reliable quantum yield. [g] Too weak for reliable spectra or lifetimes to be determined. [h] A good quality spectrum at 77 K could not be obtained for these samples, possibly due to poor solubility at low temperatures. [i] This sample showed biexponential decay kinetics, with the relative weightings of 30:70.

A number of common features within the series, as well as several trends, emerge from these results:

(i) The emission maxima are in the red region of the spectrum, in the range 600–700 nm (Figure 5), much lower in energy than the lowest-energy absorption maxima of Figure 4. They have similar values in EPA glass at 77 K (Figure 6).

(ii) The luminescence lifetimes are of the order of hundreds of nanoseconds to a few microseconds at room temperature, increasing to tens of microseconds in glassy solution at 77 K.

(iii) Within each of the three series of complexes (**1-X**, **2-X** and **3-X**), the emission energy decreases in the order I > Br > Cl (e.g., as shown for series **2-X** in Figure 7).

(iv) Within each of these three series of complexes, the iodo complexes are the brightest emitters in the solid state and the chloro the weakest; i.e., Φ_{lum} values decrease in the order I > Br > Cl. The values for the iodo complexes are of the order of 10^{-2}.

(v) Similarly, within each of the three series of complexes, the luminescence lifetimes (τ) decrease in the order I > Br > Cl.

(vi) Considering the effect of benzannulation, it can be seen from the series **1-I**, **2-I** and **3-I** that *a red shift is observed on going from the phenanthridine complexes to the corresponding quinoline complex, despite the more extended conjugation in the former* (Figures 5 and 6). The same is true for the series **1-Br**, **2-Br** and **3-Br** (and probably also for the chloro complexes, although the weakness of their emission and resulting poor spectra make the analysis unreliable).

Taken together, points (i) and (ii) strongly suggest that the emission emanates from an excited state of triplet character. The very large difference in energy between the lowest-energy absorption band and the emission band is typical of phosphorescence from a triplet state, formed indirectly following initial population of a spin-allowed singlet state through light absorption. The emission lifetimes are too long to be prompt fluorescence, but are typical of phosphorescence in which the spin selection rule has been somewhat relaxed through the effect of spin-orbit coupling. On the other hand, it is also possible that there is a thermally activated delayed fluorescence (TADF) component to the emission. As discussed in the introduction, some related copper(I) complexes have small S_1–T_1 energy gaps, allowing thermally repopulation of the singlet and hence to fluorescence but with a lifetime determined by that of the triplet state. [16] A shift in the emission maximum to lower energies upon cooling is typically a signature of TADF. For

the current set of complexes, the lack of room temperature emission in solution prohibits a direct comparison of λ_{em} with that in the low-temperature glass. Use of the solid-state room temperature data has to be treated with caution, since packing effects can significantly influence the emission properties. Notwithstanding, it can be seen that the emission maxima of, for example, the iodo complexes are displaced to longer wavelengths at 77K, suggesting that TADF may possibly be involved at room temperature.

The observed decrease in the emission energy in the order I > Br > Cl, noted in point (iii), is consistent with the proposed $^3\{d_{Cu}/p_X \rightarrow \pi^*_{N\wedge P}\}$, or ^{3}(M+X)LCT, charge-transfer assignment: the HOMO will be highest in energy for X = Cl and lowest for X = I, according to the order of ligand-field strengths of the halogens, Cl > Br > I. Such a trend has been observed previously in related halide-containing Cu(I) complexes.[22-23]

The observation that the most intense emitters (the iodo member of each family) are also the longest-lived suggests that differing rates of non-radiative decay processes may be key to the halide-dependent trends (iv) and (v). If one makes the assumption that the emitting state is formed with unitary efficiency, and therefore that the radiative rate constant $k_r = \Phi / \tau$, the values of k_r can be estimated from the experimentally-measured parameters, and hence also the rate constant of non-radiative decay processes $k_{nr} = (\tau^{-1} - k_r)$. The values thus calculated, where possible (Table 2), suggest that the trend to decreasing lifetimes and lower efficiencies in the order I > Br > Cl is due primarily to an increase in the rate of non-radiative decay k_{nr} in the order I < Br < Cl. Such an effect may in part be due to the decreasing excited state energy (lowest for chloro), in line with the

so-called 'energy gap law'. Typically, for compounds with a common type of excited state and in the absence of deactivation processes involving higher-lying states, k_{nr} should increase as the excited state energy decreases, owing to the increased probability of intramolecular energy transfer into high-energy vibrational modes within the molecule. Detailed quantitative treatments indicate that a logarithmic dependence may be anticipated,[24] as observed in some classic studies with Ru(II) and Pt(II) complexes, for example.[25-29] In the present instance, a plot of {ln k_{nr}} versus the excited-state energy (estimated from λ_{max}) reveals a quite convincing linear relationship (Figure 8).

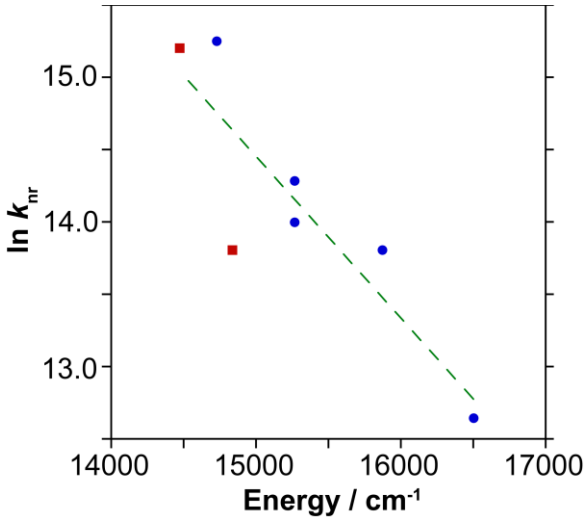

Figure 8. Plot of ln k_{nr} versus the emission energy as estimated from λ_{max} in the solid-state spectra. Data points for phenanthridine complexes are shown as blue circles; quinoline complexes as red squares. The dashed green line is the best linear fit using *all* data points.

The rate constant data suggest that an additional contribution to the trend of more efficient emission for the iodo complexes arises from an increase in the k_r value in the

order Cl < Br < I. Such a trend may be a reflection of the increasing spin-orbit coupling (SOC) constants in the same order. One caveat to this analysis is that we assume, as noted above, that the emitting state is formed with unitary efficiency in each case. This assumption relies on the rate constant of intersystem crossing (ISC) from the singlet manifold to the emissive triplet state being much faster than other deactivation pathways of the singlet. There is no evidence of any higher energy fluorescence emission in the spectra, and so the assumption may be a good approximation, but the higher SOC of iodine should also facilitate ISC. Previous work with dicopper(I)-NHC-picolyl complexes has indicated the potential importance of cuprophilic interactions in promoting phosphorescence through enhanced SOC.[30] However, the crystal structures of **2-I** and **3-I** have d_{Cu-Cu} of 2.708Å and 2.723Å, respectively, which are approximately 0.2 Å longer than the d_{Cu-Cu} observed with the dicopper(I)-NHC-picolyl complexes, and so such an effect is unlikely to play a significant role in the present complexes.

Finally, we turn to point (vi), namely the counter-intuitive observation that the quinoline complexes emit at lower energy than the phenanthridine analogues, despite the less extended π system, and contrary to the trend observed in absorption. Some insight into this trend can be gleaned from the corresponding ligands. As mentioned earlier, **L1** and **L2** display a series of lower-energy absorption bands than **L3**, indicating that the energy E_S of the lowest-lying *singlet* state of the phenanthridine ligands is lower than for the quinoline. This is reproduced in TD-DFT calculations of **2-I** and **3-I** (*vide infra*). The opposite conclusion, however, applies to the lowest-lying *triplet* states, again reproduced by TD-DFT. Inspection of the well-defined (0, 0) bands in the phosphorescence spectra of **L1** and 8-bromoquinoline (as a model for **L3** which gave a less well-resolved

spectrum) at 77 K reveals that their triplet energies E_T are approximately 21460 and 20940 cm^{-1} respectively (Figure S10). Indeed, the same trend is observed in unsubstituted phenanthridine and quinoline: E_T = 22050 and 21850 cm^{-1} respectively; *cf.* E_S = 28590 and 31850 cm^{-1} respectively.[31-32] Although we are not aware of any detailed theoretical studies into the trend in E_T versus E_S for such aromatics, there is some consensus in the literature that formation of the triplet state of arenes is accompanied by considerable distortion, for example in benzene, leading to D_{2h} symmetry where two C–C bonds are significantly lengthened relative to the ground state and four are shortened.[33-36] It then becomes clear why benzannulation (as in phenanthridine versus quinoline) might *destabilize* the triplet state, since the electronically desirable distortion may be inhibited.

Density Functional Theory (DFT) and Time-Dependent (TD-DFT) calculations

To gain further insight into the electronic structure of the Cu_2X_2 complexes, DFT calculations were carried out at the B3LYP level of theory, focusing on the iodo complexes from which emission was observed to be strongest. As emission is only observed in the solid state, the basis set was selected based on optimization of the calculated geometries to match the solid-state structures, focusing on bond lengths, angles and the conformation of the $Cu_2(\mu\text{-}I)_2$ core (diamond core vs. butterfly; see SI for full description of geometry optimization). The two conformers (diamond cores vs. butterfly) of **3-I** are very close in energy, with the butterfly motif 1.4 kJ/mol more stable than the diamond core. This suggests that both conformers can exist at room temperature in equilibrium. The extra stability in the butterfly structure could result from Cu···Cu

orbital (d_z^2 and p_z) interactions modulated by several factors such as the nature of the *P^N* ligands, the bridging halides,[37-38] and also possibly from solvent interactions, as seen in the preference for butterfly structures upon solvent inclusion in the crystal lattice (see Figure S8). To directly elucidate the impact of benzannulation, we were most curious to compare complexes **2-I** and **3-I**, which differ by formal addition of a butadiene fragment at the 2,3-position of the quinolinyl moiety in **3-I**. Basis sets 6-31G(d,p) on H, C, N, P; m6-31G(d) on Cu; and LANL2DZ on halides were found to most closely reproduce parameters from the solid-structure of **3-I** (Table S1) and **2-I** (Table S2). MOs of both complexes were calculated, with the isosurfaces of the frontier orbitals shown in Figure 9.

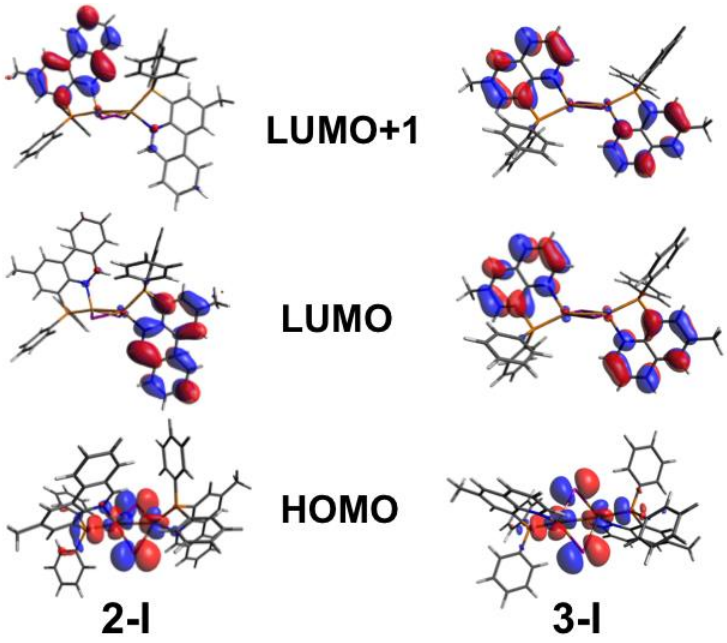

Figure 9. HOMO, LUMO and LUMO+1 diagrams for **2-I** and **3-I** (isovalue = 0.03).

Contour curves of the frontier MOs for the optimized ground state geometry are consistent with related *P^N* supported Cu_2X_2 dimers.[18, 21, 39] The HOMOs of both **2-I** and **3-I** are composed mainly of metal and halide orbital contributions, with minor contributions from the phosphorus (Table S3-S5). In the case of the planar diamond core of **3-I**, the Cu(I) centers equally contribute ~25% to the HOMO, while the iodides only contribute ~15% each. Minor contributions (~6% each) are also observed from both phosphorus centers. This is not the case for **2-I**, where for the asymmetric butterfly structure, one phosphorus contributes significantly more than the other to the HOMO (~1% vs 11%). Contributions from the two Cu atoms are also not the same (~20% vs. 33%). The asymmetry in the atomic contributions likely results from the puckering of the molecule to the butterfly structure that is observed in the solid state. Similar to pyridinyl analogs,[18, 21, 39] the LUMO/LUMO+1 of **2-I** and **3-I** are both localized on the aromatic *N*-heterocyclic quinoline or phenanthridine moieties in the excited states. For **3-I**, these two virtual orbitals are the in-phase and out-of-phase combinations of the π^* orbital framework of the two quinoline arms. In the non-centrosymmetric **2-I**, the LUMO is calculated to represent one phenanthridine ligand arm π^* orbital framework and the LUMO+1 the other, with the LUMO-containing phenanthridine ligand arm closer to the Cu_2I_2 core.

TD-DFT calculations for both **2-I** and **3-I** reveal that the transitions with the largest oscillator strengths in the low-energy region of the calculated absorption spectra have either LUMO←HOMO (**2-I**: transition 3, 69%) or LUMO+1←HOMO (**3-I**: transition 2, 49%) character. The calculated HOMOs for both **2-I** and **3-I** are localized almost entirely on the Cu_2X_2 cores, while the LUMO for **2-I** and LUMO+1 for **3-I** are

composed of the N-heterocycle π* orbitals of either the phenanthridinyl or quinolinyl moieties, supporting the (d_{Cu}+p_{halide})-to-π* charge-transfer assignment to the low energy transitions.

Comparing the frontier MO energies (Table 3), the HOMO and LUMO of **2-I** are both destabilized from their positions in the smaller **3-I**, but the occupied MO only to a small extent. The LUMO destabilization is mirrored in the electrochemistry of **2-X** and **3-X**. While the reduction of these compounds is irreversible, the LUMO energy can be estimated by the relative peak on-set ($E_{red,onset}$) which, for example, is shifted cathodically for **2-Br** ($E_{red,onset}$ ~ -2.1 V vs $FcH^{0/+}$) compared with **3-Br** ($E_{red,onset}$ ~ -2.0 V; Figure S11). In their analysis of Pt(II) complexes with bis(2-pyridylimino)isoindole (BPI) and benzannulated ligand analogs, Hanson *et al.* noted that the HOMO of a 1,3-butadiene fragment has appropriate symmetry to act as an effective electron-donating group to the LUMO of the isoindole of BPI, and that the destabilization is due largely to this effect on the LUMO, as opposed to a significant influence on the HOMO.[7] The orbital contributions to the frontier orbitals of **3-I** (Figure 9) similarly reveal that the LUMO/LUMO+1 (but not the HOMO) present lobal density of the appropriate symmetry at the site of benzannulation to interact with the HOMO of a 1,3-butadiene moiety.

This results in an increase in the calculated HOMO-LUMO gap, which does not by itself explain the appearance of additional low energy absorptions in the experimental UV-Vis spectrum. As noted earlier, the additional low energy bands in the phenanthridine-containing systems are associated with the phenanthridine unit itself. The lowest-energy bands that contribute to the long wavelength tail are presumably CT bands,

with orbital parentage as shown in Figure 9. However, as these bands form a long, unresolved tail, we hesitate to precisely compare the band positions of these lowest energy absorptions. Comparing the energies of the lowest lying singlet states obtained from the TD-DFT calculations, as predicted from the absorption spectra, the energy of the lowest lying singlet state, $E(S_1)$, for **2-I**, which boasts a larger π system, was calculated to be *lower* than the corresponding $E(S_1)$ for the quinoline congener **3-I**. The geometry of each ground state was then re-optimized as a triplet to give the geometry and free energy of the lowest lying triplet states (T_1). As observed in the emission spectra, the energy of the lowest-lying triplet states, $E(T_1)$, was found to be lower for **3-I**, in contradiction to the ordering of $E(S_1)$ (Figure S12).

Table 3. Calculated orbital energies for **2-I** and **3-I**[a]

Complex	E(HOMO)/eV	E(LUMO)/eV	E(LUMO+1/eV	$\Delta E_{HOMO-LUMO}$ /eV	$\Delta E_{HOMO-LUMO+1}$ /eV
2-I	-5.828	-0.530	-0.523	5.298	5.305
3-I	-5.828	-0.513	-0.480	5.315	5.348

[a] TD-DFT: CAM-B3LYP/6-31G(d,p) on H, C, N, P; m6-31G(d) on Cu; and LANL2DZ on I

Whilst it is not possible to say whether the trend of an increasing gap between the frontier orbitals is reflected in the absorption spectra, owing to the weak and broad nature of the long wavelength absorption tails to which the CT bands probably contribute, it is clear that the calculated trend *is* reproduced in the emission maxima of the complexes (*vide supra*, Figure 6). TD-DFT analysis revealed that, as observed for the proligands **L2** and **L3**, while the lowest lying singlet state of the phenanthridine-containing complex **2-I** is lower in energy than for the more compact π-system of the quinoline-containing **3-I**, the opposite is true for the lowest lying *triplet* states (Figure S12). Thus, **2-I** is calculated

to have a larger singlet-triplet gap and a higher energy emission maximum, despite an increase in conjugation compared with **3-I**.

Comparing the optimized geometries of the ground state (S_0) and first excited triplet state (T_1) of **2-I** and **3-I** reveals structural changes that accompany emission (Figure 10). Larger differences between ground-state (GS) and excited-state (ES) geometries are generally associated with larger Stokes shifts between emission and absorption energies.[40] The root-mean-squared deviations, calculated from overlaying the S_0 and T_1 structures (**2-I**: 1.321 Å, **3-I**: 1.551; Figure S13), are consistent with bigger structural differences for the smaller quinolinyl-based system. In both ground-state structures, the two Cu centers are found in approximate trigonal pyramidal environments, with nearly identical τ_4 indices (a useful geometric parameter for evaluating the geometry of four-coordinate complexes[41]) of 0.86/0.87 (**2-I**) and 0.86/0.86 (**3-I**) representative of tetrahedral geometries distorted towards trigonal pyramidal environments; a τ_4 value of 1.00 represents an ideal tetrahedral geometry, while 0.00 represents a square-planar environment and 0.85 a trigonal pyramidal (C_{3v}) setting.[41] In their T_1 excited states, the Cu centers in both complexes experience nearly identical "rocking" distortions[42] towards see-saw-like (C_{2v}) geometries as the Cu_2I_2 core becomes increasingly bent (τ_4 in T_1 geometries **2-I**: 0.66/0.80; **3-I**: 0.66/0.80). Thus, the more significant GS-ES geometrical distortion for **3-I** is not rooted in changes to the bond angles and coordination geometry around copper. Changes observed in the Cu-Cu and I-I bond distances are different, with a contraction of 0.08 Å and 0.38 Å, respectively, as **3-I** puckers into a butterfly structure in the T_1 state, with significant canting of the *P^N* ligand units with respect to one

another. In comparison, the Cu-Cu and I-I distances in **2-I** contract to a smaller degree (0.04 Å and 0.32 Å, respectively), as the optimized ground-state geometry of **2-I** is already bent into a butterfly-type structure.

The different extent of change to the relative orientation of the two *P^N* ligands in **3-I** vs **2-I** can be quantified by comparing P1-Cu1-Cu2/Cu1-Cu2-P2 (S_0: 153.9/153.9; T_1: 163.3/116.0) and N1-Cu1-Cu2/Cu1-Cu2-N2 (S_0: 122.5/122.5; T_1: 111.0/156.2) bond angles; these change by 38°/9° and 34°/13°, respectively, which represent significant GS-ES perturbations for **3-I**. In comparison, the same angles in **2-I** are distorted to a much smaller extent, 19°/6° and 14°/5°, respectively (P1-Cu1-Cu2/Cu1-Cu2-P2 S_0: 169.5/134.4; T_1: 163.1/115.1 and N1-Cu1-Cu2/Cu1-Cu2-N2 S_0: 142.2/106.9; T_1: 112.2/156.6). Thus, the ability of the phenanthridinyl *P^N* ligand to resist reorientation in **2-I** compared to **3-I** appears to play a role in limiting distortion in the excited state.

Looking more closely at the *N*-heterocyclic moieties, the C_5N sub-unit in the quinolinyl moiety in **3-I** is observed to distort significantly compared with the benzannulated C_5N sub-unit in the phenanthridinyl moiety of the ligand in **2-I** (Figure S14). As noted for the aromatic *N*-heterocycles themselves, the higher energy triplet state of **2-I** is also likely due to inhibition of the electronically desirable distortion for **2-I** compared with **3-I**. A similar observation has been made for cyclometallated Pt complexes with extended π-systems.[5] In that work, the extent of π-conjugation in aromatic *C^N* ligand was found to also *not* correspond with the observed trends in emission energies, and was rationalized in terms of structural distortions that occur upon cyclometalation matching distortions that stabilized the molecules' triplet states. While

the energy cost of geometry relaxation of the T_1 state to the S_0 state has been previously estimated by calculating the corresponding relaxation energy (λ_T),[43] the λ_T (Table S6) values calculated for **2-I** (0.390 eV) and **3-I** (0.391 eV), are very similar. Nevertheless, the observed and measurable geometric changes are consistent with the phenanthridinyl *P^N* ligands enforcing an excited state geometry more similar to the ground state geometry in **2-I** than for the smaller quinolinyl analogs **3-I**, with a commensurately smaller resulting Stokes shift.

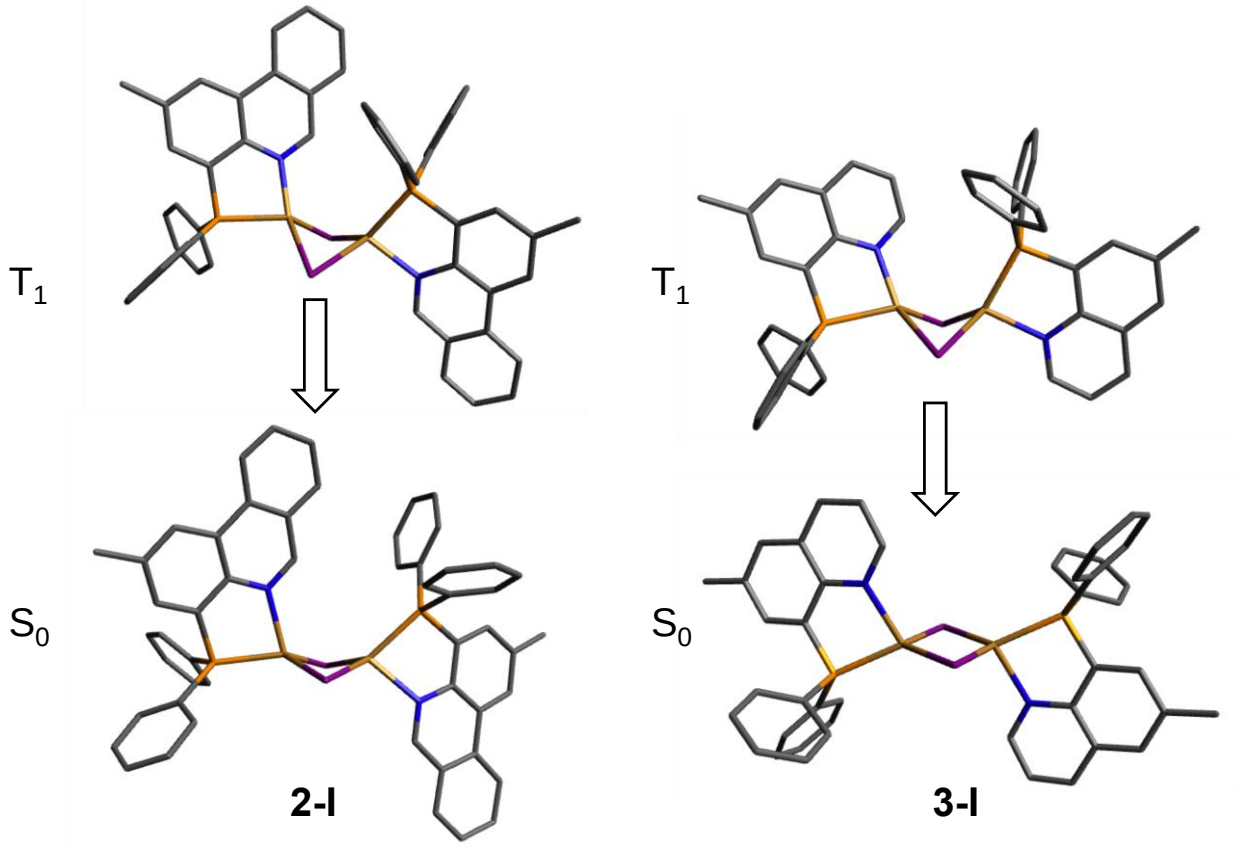

Figure 10. Comparison of optimized structures for T_1 and S_0 states of **2-I** and **3-I**.

CONCLUSION

The design of new emissive molecules based on relatively low-cost copper is an important target in sustainable materials chemistry.[44-47] To fully realize the potential of luminescent Cu coordination complexes, the ability to tune emission wavelengths based on molecular structure is critical. While ligand benzannulation and the resulting extension of a molecule's π-system is often used to red-shift absorption and emission,[6] understanding the mechanism underlying changes in a molecule's electronic structure both in the ground state and excited (emissive) states can allow for both red and blue shifts.[5, 7] Despite appearing to represent a simple extension of a quinoline π system, the incorporation of phenanthridine (3,4-benzoquinoline) into ligand frameworks results in a counter-intuitive blue shift of emission maximum, assigned as phosphorescence from metal-affected, ligand-centered triplet states. The asymmetry of benzannulation in phenanthridine both renders it a more potent and less sterically encumbered donor, and in this case, results in a destabilization of the emissive triplet state relative to the more compact π system of the quinoline derivative. The applicability of this model in similarly perturbing excited state energies of Pt[5] and Ir[6] based emitters is currently underway.

EXPERIMENTAL SECTION

Unless otherwise stated, all air sensitive manipulations were carried out inside an inert-atmosphere glove box (N_2) or using standard Schlenk techniques (Ar). 2,6-Dibromoaniline (AK Scientific), *N*-iodosuccinimide (AK Scientific), *p*-toluidine (Alfa Aesar), *N*-bromosuccinimide (Alpha Aesar), 2-formylphenyl boronic acid (Combi Blocks), $Pd(PPh_3)_4$ (Alfa Aesar), Na_2CO_3 (Alfa Aesar), chlorodiphenylphosphine (VWR), CuBr (Aldrich), CuI (Aldrich) and CuCl (Acros) were purchased from commercial

suppliers and used as received. 2-Bromo-4-methylaniline,[48] 6-bromo-2-iodo-4-methylaniline,[9] 4-bromo-2-methylphenanthridine,[9] 8-bromo-6-methylquinoline,[48] 4-diphenylphosphinophenanthridine[8] (**L1**) and {(4-diphenylphosphino)phenanthridine}CuBr (**1-Br**)[8] were synthesized following published procedures. Organic solvents were dried over appropriate reagents and deoxygenated prior to use, with the exception of 1,2-dimethoxyethane and water, which were simply degassed. NMR spectra were recorded on a Bruker Avance 300 MHz or Bruker Avance-III 500 MHz spectrometer as noted. Elemental analyses were performed by Canadian Microanalytical Service Ltd., Delta, BC (Canada).

Synthesis of 4-diphenylphosphino-2-methylphenanthridine (L2)

4-Bromo-2-methylphenanthridine (2.18 g, 8.00 mmol) was dissolved in diethylether (6 mL) and cooled to -78 °C. A solution of *sec*-butyllithium in cyclohexane (1.6 M, 6.4 mL, 8.00 mmol) was added drop-wise over a period of 15 min. The mixture was stirred for additional 6 h at this temperature, following which a solution of chlorodiphenylphosphine (1.78 g, 8.00 mmol) in diethylether (6 mL) was added drop-wise. The reaction mixture was allowed to warm to room temperature overnight at which point a white precipitate was observed. The volatiles were removed under reduced pressure and the solid residue was dissolved in dichloromethane (40 mL) and filtered through a small plug of Celite. The filtrate was dried under vacuum to give a light brown solid, which was washed with degassed ethanol (50 mL). Yield = 1.91 g (63%). ^{1}H NMR ($CDCl_3$, 300 MHz, 22 °C): δ 9.19 (s, 1H, $^{phen}C_{Ar}$-*H*), 8.59 (d, J_{HH} = 9 Hz, 1H, $^{phen}C_{Ar}$-*H*), 8.37 (s, 1H, $^{phen}C_{Ar}$-*H*), 7.97 (d, 1H, J_{HH} = 6 Hz, $^{phen}C_{Ar}$-*H*), 7.81 (m, 1H, $^{phen}C_{Ar}$-*H*), 7.65

(m, 1H, $^{phen}C_{Ar}$-*H*), 7.41-7.32 (overlapped m, 10H, PC_{Ar}-*H*), 7.00 (br, 1H, $^{phen}C_{Ar}$-*H*), 2.48 ppm (s, 3H, C_{Me}-*H*). $^{13}C\{^1H\}$ NMR ($CDCl_3$, 75 MHz, 22 °C): δ 151.8 (br, J_{CP} = 2 Hz, ^{phen}C=N), 144.4 (d, J_{CP} = 17 Hz, $^{phen}C_{Ar}$), 138.6 (d, J_{CP} = 12 Hz, $^{phen}C_{Ar}$), 137.9 (d, J_{CP} = 11 Hz, PC_{Ar}), 136.8 ($^{phen}C_{Ar}$Me), 134.8 ($^{phen}C_{Ar}$H), 134.2 (d, J_{CP} = 20 Hz, PC_{Ar}H), 132.3 (d, J_{CP} = 2 Hz, $^{phen}C_{Ar}$), 130.7 ($^{phen}C_{Ar}$H), 128.8 ($^{phen}C_{Ar}$H), 128.4 (d, J_{CP} = 5 Hz, PC_{Ar}H), 128.3 (PC_{Ar}H), 127.5 ($^{phen}C_{Ar}$H), 126.5 (br, $^{phen}C_{Ar}$), 123.6 (d, J_{CP} = 2 Hz, $^{phen}C_{Ar}$) 122.8 ($^{phen}C_{Ar}$H), 122.1 ($^{phen}C_{Ar}$H), 22.2 ppm (C_{Me}). $^{31}P\{^1H\}$ NMR ($CDCl_3$, 121 MHz, 22 °C): δ -13.6 ppm (s).

Synthesis of 8-diphenylphosphino-6-methylquinoline (L3)

This compound was synthesized following the procedure detailed for **L2**, using 8-bromo-6-methylquinoline (1.75 g, 8.00 mmol) and *sec*-butyllithium (1.6 M, 6.4 mL, 8.00 mmol) in Et_2O, followed by addition of chlorodiphenylphosphine (1.78 g, 8.00 mmol). The product was isolated as an off-white solid. Yield = 1.76 g (67%). ^1H NMR ($CDCl_3$, 300 MHz, 22 °C): δ 8.79 (m, 1H, $^{quin}C_{Ar}$-*H*), 8.06 (d, 1H, $^{quin}C_{Ar}$-H, J_{HH} = 9 Hz), 7.57 (s, 1H, $^{quin}C_{Ar}$-*H*), 7.36-7.27 (overlapped m, 11H, PC_{Ar}-*H* + $^{quin}C_{Ar}$-*H*), 6.93 (br, 1H, $^{quin}C_{Ar}$-*H*), 2.38 ppm (s, 3H, C_{Me}-*H*). $^{13}C\{^1H\}$ NMR ($CDCl_3$, 75 MHz, 22 °C): δ 149.0 (d, J_{CP} = 1.5 Hz, ^{quin}C=N), 148.4 (d, J_{CP} = 17 Hz, $^{quin}C_{Ar}$), 138.2 (d, J_{CP} = 13 Hz, $^{quin}C_{Ar}$), 137.7 (d, J_{CP} = 11 Hz, PC_{Ar}), 136.5 ($^{quin}C_{Ar}$H), 136.4 ($^{quin}C_{Ar}$Me), 135.5 (m, J_{CP} = 2 Hz, $^{quin}C_{Ar}$H), 134.3 (d, J_{CP} = 20 Hz, PC_{Ar}H), 128.5 (d, J_{CP} = 7 Hz, PC_{Ar}H), 128.4 (PC_{Ar}H), 128.1 (br, J_{CP} = 2 Hz, PC_{Ar}), 127.8 ($^{quin}C_{Ar}$H), 121.5 ($^{quin}C_{Ar}$H), 21.84 ppm (C_{Me}). $^{31}P\{^1H\}$ NMR ($CDCl_3$, 121 MHz, 22 °C): δ -14.9 ppm (s).

Representative synthesis of Cu_2X_2 complexes:

All halide-bridged Cu(I) complexes were prepared via an analogous procedure to the preparation of **1-Br**[8]: a solution of **L1**, **L2** or **L3** (0.063 mmol) in CH_2Cl_2 (3 mL) was added drop-wise to a stirring suspension of CuX (0.063 mmol) in CH_2Cl_2 (3mL). The reaction mixture was stirred overnight at room temperature. The solution was then filtered through a small plug of Celite and solid material was obtained via crystallization following slow diffusion of hexane into a dichloromethane solution. For **3-X**, single crystals suitable for X-ray diffraction were obtained via slow diffusion of diethylether into CH_2Cl_2 solutions of the complexes.

Complexes **1-I**, **2-I** and **3-I** were also prepared by grinding together the appropriate ligand and CuX precursor together with five drops of CH_3CN in a porcelain mortar and pestle, following a published procedure.[18] Specifically, solid **L1**, **L2** or **L3** (0.063 mmol) and CuI (0.063 mmol) were placed in the mortar and five drops of CH_3CN were added and the mixture was thoroughly ground with a pestle for 5 min, at which time the color of the mixture could be clearly seen to change (Figure S1). The solid was scraped from the mortar, dried under vacuum and ^1H and ^{31}P NMR spectra were collected. The NMR spectra were identical to those obtained from solution state reactions (see Figures S2-S7 and S15-S44).

1-Cl: Orange-red crystals. Yield = 0.026 g (89%). ^1H NMR ($CDCl_3$, 500 MHz, 22 °C): δ 9.05 (v br, 1H, $^{phen}C_{Ar}$-*H*), 8.83 (br, J_{HH}= 5 Hz, 1H, $^{phen}C_{Ar}$-*H*), 8.69 (br, J_{HH}= 10 Hz, 1H, $^{phen}C_{Ar}$-*H*), 7.99 (m, 1H, $^{phen}C_{Ar}$-*H*), 7.87 (m, 2H, $^{phen}C_{Ar}$-*H*), 7.76-7.71 (m, 2H, $^{phen}C_{Ar}$-

H), 7.52-7.49 (overlapped m, 4H, P*C*$_{Ar}$-*H*), 7.44-7.41 (m, 2H, P*C*$_{Ar}$-*H*), 7.36-7.33 ppm (overlapped m, 4H, P*C*$_{Ar}$-*H*). ^{13}C NMR ($CDCl_3$, 126 MHz, 22 °C): δ 156.9 (^{phen}*C*$_{Ar}$H), 145.3 (d, J_{CP} = 16 Hz, ^{phen}*C*$_{Ar}$), 135.9 (^{phen}*C*$_{Ar}$H), 133.5 (d, J_{CP} = 15 Hz, P*C*$_{Ar}$H), 133.3 (^{phen}*C*$_{Ar}$), 132.8 (^{phen}*C*$_{Ar}$H), 131.6 (d, J_{CP} = 31 Hz, P*C*$_{Ar}$), 130.4 (P*C*$_{Ar}$H), 129.9 (^{phen}*C*$_{Ar}$H), 129.3 (br, J_{CP} = 10 Hz, P*C*$_{Ar}$H), 129.0 (^{phen}*C*$_{Ar}$H), 128.3 (br, J_{CP} = 5 Hz, ^{phen}*C*$_{Ar}$H), 126.6 (^{phen}*C*$_{Ar}$), 125.9 (^{phen}*C*$_{Ar}$H), 125.6 (^{phen}*C*$_{Ar}$), 122.4 ppm (^{phen}*C*$_{Ar}$H). ^{31}P{^{1}H} NMR ($CDCl_3$, 202 MHz, 22 °C): δ -17.9 ppm (br, s). Anal. Calc. for $C_{50}H_{36}N_2P_2Cu_2Cl_2$**.**(0.5 CH_2Cl_2): C, 60.67; H, 3.79. Found: C, 60.90; H, 3.90.

1-I: Yellow crystals. Yield = 0.029 g (84%). ^{1}H NMR ($CDCl_3$, 500 MHz, 22 °C): δ 9.88 (s, 1H, ^{phen}*C*$_{Ar}$-*H*), 8.68 (d, J_{HH} = 10 Hz, 1H, ^{phen}*C*$_{Ar}$-*H*), 8.60 (d, J_{HH} = 10 Hz, 1H, ^{phen}*C*$_{Ar}$-*H*), 7.89 (m, 1H, ^{phen}*C*$_{Ar}$-*H*), 7.77-7.70 (overlapped m, 3H, ^{phen}*C*$_{Ar}$-*H*), 7.66-7.61 (overlapped m, 5H, ^{phen}*C*$_{Ar}$-*H*, P*C*$_{Ar}$-*H*), 7.36-7.28 ppm (overlapped m, 6H, P*C*$_{Ar}$-*H*). ^{13}C{^{1}H} NMR ($CDCl_3$, 126 MHz, 22 °C): δ 156.3 (d, J_{CP} = 4 Hz, ^{phen}*C*$_{Ar}$H), 145.2 (d, J_{CP} = 18 Hz, ^{phen}C$_{Ar}$), 135.8 (^{phen}*C*$_{Ar}$H), 134.1 (d, J_{CP} = 16 Hz, P*C*$_{Ar}$H), 133.4 (^{phen}*C*$_{Ar}$), 133.2 (^{phen}*C*$_{Ar}$), 132.8 (^{phen}*C*$_{Ar}$), 132.3 (^{phen}*C*$_{Ar}$H), 129.7 (P*C*$_{Ar}$H), 129.6 (^{phen}*C*$_{Ar}$H), 128.7 (d, J_{CP} = 10 Hz, P*C*$_{Ar}$H), 128.4 (^{phen}*C*$_{Ar}$H), 127.4 (d, J_{CP} = 4 Hz, ^{phen}*C*$_{Ar}$H), 127.0 (br, J_{CP} = 3 Hz, ^{phen}*C*$_{Ar}$), 125.2 (br, J_{CP} = 4 Hz, ^{phen}*C*$_{Ar}$H), 124.9 (^{phen}*C*$_{Ar}$), 122.1 ppm (^{phen}*C*$_{Ar}$H). ^{31}P{^{1}H} NMR ($CDCl_3$, 121 MHz, 22 °C): δ -28.3 ppm (br, s). Anal. Calc. for $C_{50}H_{36}N_2P_2Cu_2I_2$•($CH_2Cl_2$): C, 51.36; H, 3.21. Found: C, 51.70; H, 2.85.

2-Cl: Orange-red crystals. Yield = 0.022 g (74%). ^{1}H NMR ($CDCl_3$, 300 MHz, 22 °C): δ 8.83 (br, 1H, ^{phen}*C*$_{Ar}$-H C$_6$-*H*), 8.69 (d, J_{HH} = 8.3 Hz, 1H, ^{phen}*C*$_{Ar}$-*H*), 8.63 (s, 1H, ^{phen}*C*$_{Ar}$-

H), 8.01-7.96 (m, 1H, $^{phen}C_{Ar}$-*H*), 7.75 -7.66 (m, J_{HH} = 5.5, 4.5 Hz, 3H, $^{phen}C_{Ar}$-*H*), 7.50 – 7.42 (overlapped m, 6H, PC_{Ar}-*H*), 7.38 – 7.33 (overlapped m, 4H, PC_{Ar}-*H*), 2.66 ppm (s, 3H, C_{Me}-*H*). $^{13}C\{^{1}H\}$ NMR ($CDCl_3$, 126 MHz, 22 °C): δ 155.1 ($^{phen}C_{Ar}H$), 143.8 (d, J_{CP} = 17 Hz, $^{phen}C_{Ar}$), 138.8 ($^{phen}C_{Ar}H$), 137.2 ($^{phen}C_{Ar}$), 133.4 (br, J_{CP} = 15 Hz, P$C_{Ar}H$), 133.2 ($^{phen}C_{Ar}$), 132.5 ($^{phen}C_{Ar}H$), 131.4 (d, J_{CP} = 30 Hz, PC_{Ar}), 130.5 (P$C_{Ar}H$), 129.7 ($^{phen}C_{Ar}H$), 129.2 (d, J_{CP} = 8 Hz, P$C_{Ar}H$), 128.9 ($^{phen}C_{Ar}H$), 126.5 ($^{phen}C_{Ar}H$), 125.9 ($^{phen}C_{Ar}$), 125.5 ($^{phen}C_{Ar}H$), 122.4 ($^{phen}C_{Ar}H$), 22.2 ppm (C_{Me}). $^{31}P\{^{1}H\}$ NMR ($CDCl_3$, 121 MHz, 22 °C): δ -17.2 ppm (br, s). Anal. Calc. for $C_{52}H_{40}N_2P_2Cu_2Cl_2$: C, 65.55; H, 4.23. Found: C, 65.02; H, 4.27.

2-Br: Orange crystals. Yield = 0.026 g (81%). ^{1}H NMR ($CDCl_3$, 500 MHz, 22 °C): δ 9.36 (br s, 1H, $^{phen}C_{Ar}$-H), 8.61 (d, J_{HH} = 8.6 Hz, 1H, $^{phen}C_{Ar}$-*H*), 8.52 (s, 1H, $^{phen}C_{Ar}$-*H*), 7.92-7.89 (m, 1H, $^{phen}C_{Ar}$-*H*), 7.73 (d, J_{HH} = 7.8 Hz, 1H, $^{phen}C_{Ar}$-*H*), 7.67 – 7.55 (overlapped m, 6H, $^{phen}C_{Ar}$-*H*, PC_{Ar}-*H*), 7.41 – 7.32 (overlapped m, 6H, PC_{Ar}-*H*), 2.62 ppm (s, 3H, C_{Me}-*H*). $^{13}C\{^{1}H\}$ NMR ($CDCl_3$, 126 MHz, 22 °C): δ 154.9 ($^{phen}C_{Ar}H$), 143.7 (d, J_{CP} = 17 Hz, $^{phen}C_{Ar}$), 137.9 (br, $^{phen}C_{Ar}H$), 136.9 ($^{phen}C_{Ar}$), 133.8 (d, J_{CP} = 15 Hz, P$C_{Ar}H$), 132.5 (d, J_{CP} = 5 Hz, $^{phen}C_{Ar}H$), 132.3 (br, $^{phen}C_{Ar}$), 130.1 (P$C_{Ar}H$), 129.8 ($^{phen}C_{Ar}H$), 129.0 (br, J_{CP} = 10 Hz, P$C_{Ar}H$), 128.6 ($^{phen}C_{Ar}H$), 126.8 ($^{phen}C_{Ar}$), 125.3 ($^{phen}C_{Ar}$), 125.2 (d, J_{CP} = 4 Hz, $^{phen}C_{Ar}H$), 122.2 ($^{phen}C_{Ar}H$), 22.2 ppm (C_{Me}). $^{31}P\{^{1}H\}$ NMR ($CDCl_3$, 121 MHz, 22 °C): δ -22.5 ppm (br, s). Anal. Calc. for $C_{52}H_{40}N_2P_2Cu_2Br_2$: C, 59.95; H, 3.87. Found: C, 59.92; H, 3.90.

2-I: Yellow crystals. Yield = 0.024 g (68%). ^{1}H NMR ($CDCl_3$, 300 MHz, 22 °C): δ 9.75 (s, 1H, $^{phen}C_{Ar}$-*H*), 8.60 (d, J_{HH} = 9 Hz, 1H, $^{phen}C_{Ar}$-*H*), 8.47 (s, 1H, $^{phen}C_{Ar}$-*H*), 7.91-7.86 (m, 1H, $^{phen}C_{Ar}$-*H*), 7.75 (d, J_{HH} = 6 Hz, 1H, $^{phen}C_{Ar}$-*H*), 7.67-7.55 (overlapping m, 6H, $^{phen}C_{Ar}$-*H*, PC_{Ph}-*H*), 7.39-7.28 (overlapping m, 6H, $^{phen}C_{Ar}$-*H*, PC_{Ph}-*H*), 2.59 ppm (s, 3H, C_{Me}-*H*). $^{13}C\{^{1}H\}$ NMR ($CDCl_3$, 126 MHz, 22 °C): δ 155.4 ($^{phen}C_{Ar}$-*H*), 143.7 (d, J_{CP} = 18 Hz, $^{phen}C_{Ar}$), 137.5 ($^{phen}C_{Ar}$), 137.0 ($^{phen}C_{Ar}$-*H*), 134.1 (d, J_{CP} = 16 Hz, PC_{Ar}-*H*), 133.2 ($^{phen}C_{Ar}$), 132.5 ($^{phen}C_{Ar}$-*H*), 132.0 (PC_{Ar}), 129.7 ($^{phen}C_{Ar}$), 129.6 ($^{phen}C_{Ar}$-*H*), 128.7 (d, J_{CP} = 9 Hz, PC_{Ar}-*H*), 128.2 (PC_{Ar}-*H*), 127.1 ($^{phen}C_{Ar}$-*H*), 125.1 ($^{phen}C_{Ar}$), 125.0 ($^{phen}C_{Ar}$), 124.9 ($^{phen}C_{Ar}$), 122.0 ($^{phen}C_{Ar}$-*H*), 22.1 ppm (C_{Me}). $^{31}P\{^{1}H\}$ NMR ($CDCl_3$, 202 MHz, 22 °C): δ -27.8 ppm (br, s). Anal. Calc. for $C_{52}H_{40}N_2P_2Cu_2I_2$•($CH_2Cl_2$): C, 54.99; H, 3.55. Found: C, 54.45; H, 3.60.

3-Cl: Red crystals. Yield = 0.019 g (70%). ^{1}H NMR ($CDCl_3$, 300 MHz, 25 °C): 8.38 (m-overlapped, J_{HH} = 9, 3 Hz, 1H, $^{quin}C_{Ar}$-*H*), 8.33 (br s - overlapped, 1H, $^{quin}C_{Ar}$-*H*), 7.91 (s, 1H, $^{quin}C_{Ar}$-*H*), 7.73 (br, J_{HH} = 3 Hz, 1H, $^{quin}C_{Ar}$-*H*), 7.45 – 7.31 (overlapping m, 11 H, $^{quin}C_{Ar}$-*H*, PC_{Ph}-*H*), 2.57 ppm (s, 3H, C_{Me}-*H*). $^{13}C\{^{1}H\}$ NMR ($CDCl_3$, 75 MHz, 22 °C): δ 151.3 ($^{quin}C_{Ar}$-*H*), 147.8 (d, J_{CP} = 18 Hz, $^{quin}C_{Ar}$), 139.9 ($^{quin}C_{Ar}$-*H*), 138.5 ($^{quin}C_{Ar}$-*H*), 138.3 ($^{quin}C_{Ar}$-*H*), 133.2 (br, J_{CP} = 14 Hz, PC_{Ar}-*H*), 131.3 (d, J_{CP} = 32 Hz, PC_{Ar}), 130.9 ($^{quin}C_{Ar}$), 130.5 ($^{quin}C_{Ar}$-*H*), 129.3 (PC_{Ar}-*H*), 129.2 (PC_{Ar}-*H*), 123.0 (PC_{Ar}-*H*), 21.8 ppm (C_{Me}). $^{31}P\{^{1}H\}$ NMR ($CDCl_3$, 121 MHz, 22 °C): δ -18.2 ppm (br, s). Anal. Calc. for $C_{44}H_{36}N_2P_2Cu_2Cl_2$: C, 61.98; H, 4.26. Found: C, 61.55; H, 4.01.

3-Br: Orange crystals. Yield = 0.023 g (79%). ^{1}H NMR ($CDCl_3$, 300 MHz, 25 °C): δ 8.94 (br, s, 1H, $^{quin}C_{Ar}$-*H*), 8.24 (d, J_{HH} = 6 Hz, 1H, $^{quin}C_{Ar}$-*H*), 7.78 (s, 1H, $^{quin}C_{Ar}$-*H*), 7.67 (m, J_{HH} = 9, 3 Hz, 1H, $^{quin}C_{Ar}$-*H*) 7.54-7.48 (overlapping m, 4H, $^{quin}C_{Ar}$-*H*, PC_{Ar}-*H*), 7.44-7.29 (overlapping m, 7H, PC_{Ar}-*H*), 2.53 ppm (s, 3H, C_{Me}-*H*). $^{13}C\{^{1}H\}$ NMR ($CDCl_3$, 75 MHz, 22 °C): δ 151.3 (d, J_{CP} = 4 Hz, $^{quin}C_{Ar}$-*H*), 147.5 (d, J_{CP} = 17 Hz, $^{quin}C_{Ar}$), 139.3 ($^{quin}C_{Ar}$-*H*), 137.6 ($^{quin}C_{Ar}$-*H*), 137.5 ($^{quin}C_{Ar}$-*H*), 133.7 (d, J_{CP} = 17 Hz, PC_{Ar}-*H*), 132.1 (d, J_{CP} = 30 Hz, PC_{Ar}), 130.2 ($^{quin}C_{Ar}$), 130.1 ($^{quin}C_{Ar}$), 129.0 (PC_{Ar}-*H*), 128.9 (PC_{Ar}-*H*), 122.9 (d, J_{CP} = 3 Hz, PC_{Ar}-*H*), 21.8 ppm (C_{Me}). $^{31}P\{^{1}H\}$ NMR ($CDCl_3$, 121 MHz, 22 °C): δ -23.7 ppm (br, s). Anal. Calc. for $C_{44}H_{36}N_2P_2Cu_2Br_2$: C, 56.12 H, 3.85. Found: C, 55.71 H, 3.84.

3-I: Orange-red crystals. Yield = 0.022 g (69%). ^{1}H NMR ($CDCl_3$, 300 MHz, 22 °C): δ 9.28 (br, 1H, $^{quin}C_{Ar}$-*H*), 8.14 (d, J_{HH} = 9 Hz, 1H, $^{quin}C_{Ar}$-*H*), 7.69 (s, 1H, $^{quin}C_{Ar}$-*H*), 7.61 – 7.56 (overlapping m, 5H, $^{quin}C_{Ar}$-*H*, PC_{Ph}-*H*), 7.37 – 7.28 (overlapping m, 7H, $^{quin}C_{Ar}$-*H*, PC_{Ph}-*H*), 2.50 ppm (s, 3H, C_{Me}-*H*). $^{13}C\{^{1}H\}$ NMR ($CDCl_3$, 75 MHz, 22 °C): δ 151.8 (d, J_{CP} = 5 Hz, $^{quin}C_{Ar}$-*H*), 147.3 (d, J_{CP} = 18 Hz, $^{quin}C_{Ar}$), 139.2 (d, J_{CP} = 3 Hz, $^{quin}C_{Ar}$-*H*), 137.1 (d, J_{CP} = 4 Hz, $^{quin}C_{Ar}$), 136.9 (d, J_{CP} = 2.2 Hz, $^{quin}C_{Ar}$-*H*), 135.5 (d, J_{CP} = 17 Hz, $^{quin}C_{Ar}$), 134.0 (d, J_{CP} = 15.7 Hz, PC_{Ph}-*H*), 133.1 (PC_{Ar}), 129.6 ($^{quin}C_{Ar}$), 128.8 ($^{quin}C_{Ph}$), 128.7 (d, J_{CP} = 15 Hz, PC_{Ar}-*H*), 122.8 (d, J_{CP} = 3 Hz, $PC_{Ar}H$), 21.7 ppm (C_{Me}). $^{31}P\{^{1}H\}$ NMR ($CDCl_3$, 121 MHz, 22 °C): δ -29.9 ppm (br, s). Anal. Calc. for $C_{44}H_{36}N_2P_2Cu_2I_2$: C, 51.03; H, 3.50. Found: C, 50.63; H, 3.48.

X-Ray Crystallography Experimental Details

X-ray crystal structure data was using collected from multi-faceted crystals of suitable size and quality selected from a representative sample of crystals of the same habit using an optical microscope. In each case, crystals were mounted on MiTiGen loops with data collection carried out in a cold stream of nitrogen (150 K; Bruker D8 QUEST ECO). All diffractometer manipulations were carried out using Bruker APEX3 software.[49] Structure solution and refinement was carried out using XS, XT and XL software, embedded within the Bruker SHELXTL suite.[50] For each structure, the absence of additional symmetry was confirmed using ADDSYM incorporated in the PLATON program.[51] CCDC Nos. 1811419-1811424 contain the supplementary crystallographic data for this paper. The data can be obtained free of charge from The Cambridge Crystallographic Data Centre via www.ccdc.cam.ac.uk/structures.

Crystal structure data for **2-Cl**: X-ray quality crystals were grown following diffusion of diethylether vapor into CH_2Cl_2 at room temperature. Crystal structure parameters: $C_{52}H_{40}Cl_2Cu_2N_2P_2$ 952.80 g/mol, triclinic, space group *P*-1; a = 9.1636(17) Å, b = 10.448(2) Å, c = 12.101(2) Å, α = 96.098(14)°, β = 99.601(13)°, γ = 109.077(17)°, V = 1063.4(4) Å^3; Z = 1, ρ_{calcd} = 1.488 g cm^{-3}; crystal dimensions 0.310 x 0.270 x 0.100 mm; diffractometer Bruker D8 QUEST ECO CMOS; Mo K$_\alpha$ radiation, 150(2) K, $2\theta_{max}$ = 34.463°; 78831 reflections, 8169 independent (R_{int} = 0.0288), direct methods; absorption coeff (μ = 1.241 mm^{-1}), absorption correction semi-empirical from equivalents (SADABS); refinement (against F_o^2) with SHELXTL V6.1, 272 parameters, 0 restraints,

R_1 = 0.0297 ($I > 2\sigma$) and wR_2 = 0.0759 (all data), Goof = 1.024, residual electron density 0.592/−0.404 e Å^{-3}.

Crystal structure data for **2-Br**: X-ray quality crystals were grown following diffusion of diethylether vapor into CH_2Cl_2 at room temperature. Crystal structure parameters: $C_{52}H_{40}Br_2Cu_2N_2P_2$ 1041.70 g/mol, monoclinic, space group *C*2/c; a = 18.8357(10) Å, b = 14.1568(7) Å, c = 16.0421(8) Å, β = 90.953(2)°, V = 4277.1(4) Å^3; Z = 4, ρ_{calcd} = 1.618 g cm^{-3}; crystal dimensions 0.310 x 0.180 x 0.100 mm; diffractometer Bruker D8 QUEST ECO CMOS; Mo K$_\alpha$ radiation, 150(2) K, $2\theta_{max}$ = 33.213°; 82121 reflections, 8185 independent (R_{int} = 0.0588), direct methods; absorption coeff (μ = 2.978 mm^{-1}), absorption correction semi-empirical from equivalents (SADABS); refinement (against F_o^2) with SHELXTL V6.1, 272 parameters, 0 restraints, R_1 = 0.0376 ($I > 2\sigma$) and wR_2 = 0.0738 (all data), Goof = 1.079, residual electron density 0.882/−0.752 e Å^{-3}.

Crystal structure data for **2-I**: X-ray quality crystals were grown following diffusion of hexanes into CH_2Cl_2 at room temperature. Crystal structure parameters: $C_{52}H_{40}I_2Cu_2N_2P_2(CH_2Cl_2)_2$ 1305.53 g/mol, monoclinic, space group *P*2/n; a = 21.0960(18) Å, b = 10.6127(8) Å, c = 24.0691(19) Å, β = 108.277(4)°, V = 5116.9(7) Å^3; Z = 4, ρ_{calcd} = 1.695 g cm^{-3}; crystal dimensions 0.170 x 0.080 x 0.050 mm; diffractometer Bruker D8 QUEST ECO CMOS; Mo K$_\alpha$ radiation, 150(2) K, $2\theta_{max}$ = 27.582°; 108133 reflections, 11817 independent (R_{int} = 0.0926), direct methods; absorption coeff (μ = 2.348 mm^{-1}), absorption correction semi-empirical from equivalents (SADABS); refinement (against

F_o^2) with SHELXTL V6.1, 649 parameters, 0 restraints, R_1 = 0.0378 ($I > 2\sigma$) and wR_2 = 0.0749 (all data), Goof = 1.017, residual electron density 0.762/−0.937 e Å^{-3}.

Crystal structure data for **3-Cl**: X-ray quality crystals were grown following diffusion of diethylether vapor into CH_2Cl_2 at room temperature. Crystal structure parameters: $C_{44}H_{36}Cl_2Cu_2N_2P_2$ 852.67 g/mol, monoclinic, space group $P2_1/n$; a = 9.7430(6) Å, b = 15.2568(9) Å, c = 12.7931(8) Å, β = 96.112(3)°, V = 1890.8(2) Å^3; Z = 2, ρ_{calcd} = 1.498 g cm^{-3}; crystal dimensions 0.080 x 0.080 x 0.050 mm; diffractometer Bruker D8 QUEST ECO CMOS; Mo Kα radiation, 150(2) K, $2\theta_{max}$ = 27.557°; 65040 reflections, 4350 independent (R_{int} = 0.0523), direct methods; absorption coeff (μ = 1.386 mm^{-1}), absorption correction semi-empirical from equivalents (SADABS); refinement (against F_o^2) with SHELXTL V6.1, 236 parameters, 0 restraints, R_1 = 0.0328 ($I > 2\sigma$) and wR_2 = 0.0641 (all data), Goof = 1.050, residual electron density 0.380/−0.524 e Å^{-3}.

Crystal structure data for **3-Br**: X-ray quality crystals were grown following diffusion of diethylether vapor into CH_2Cl_2 at room temperature. Crystal structure parameters: $C_{44}H_{36}Br_2Cu_2N_2P_2$ 941.59 g/mol, monoclinic, space group $P2_1/n$; a = 9.8884(5) Å, b = 15.3309(8) Å, c = 12.6587(8) Å, β = 95.466(2)°, V = 1910.31(18) Å^3; Z = 2, ρ_{calcd} = 1.637 g cm^{-3}; crystal dimensions 0.330 x 0.260 x 0.220 mm; diffractometer Bruker D8 QUEST ECO CMOS; Mo Kα radiation, 150(2) K, $2\theta_{max}$ = 42.248°; 126369 reflections, 13474 independent (R_{int} = 0.0495), direct methods; absorption coeff (μ = 3.324 mm^{-1}), absorption correction semi-empirical from equivalents (SADABS); refinement (against

F_o^2) with SHELXTL V6.1, 236 parameters, 0 restraints, R_1 = 0.0315 ($I > 2\sigma$) and wR_2 = 0.0730 (all data), Goof = 1.074, residual electron density 0.731/−0.802 e Å^{-3}.

Crystal structure data for **3-I**: X-ray quality crystals were grown following diffusion of diethylether vapor into CH_2Cl_2 at room temperature. Crystal structure parameters: $C_{44}H_{36}I_2Cu_2N_2P_2$ 1035.59 g/mol, monoclinic, space group $P2_1/n$; a = 10.0569(6) Å, b = 15.2785(10) Å, c = 13.3126(9) Å, β = 103.807(2)°, V = 1986.4(2) Å^3; Z = 4, ρ_{calcd} = 1.731 g cm^{-3}; crystal dimensions 0.400 x 0.220 x 0.190 mm; diffractometer Bruker D8 QUEST ECO CMOS; Mo K$_\alpha$ radiation, 150(2) K, $2\theta_{max}$ = 40.350°; 111652 reflections, 12535 independent (R_{int} = 0.0331), direct methods; absorption coeff (μ = 2.739 mm^{-1}), absorption correction semi-empirical from equivalents (SADABS); refinement (against F_o^2) with SHELXTL V6.1, 236 parameters, 0 restraints, R_1 = 0.0318 ($I > 2\sigma$) and wR_2 = 0.0733 (all data), Goof = 1.143, residual electron density 1.542/−1.106 e Å^{-3}.

Optical Spectroscopy Measurements

The absorption spectra of the complexes were measured in solution in CH_2Cl_2 in 1 cm quartz cuvettes using a Thermo Scientific Genesys UV-vis spectrometer at room temperature. Emission spectra at 77 K were recorded in 4 mm diameter tubes held within a liquid-nitrogen-cooled quartz dewar, using a Jobin Yvon Fluoromax-2 spectrometer equipped with a Hamamatsu R928 photomultiplier tube (PMT). The spectra in the solid state were recorded by means of an integrating sphere attached to a Jobin Yvon Fluorolog instrument through optical fibres. Finely powdered samples were contained within Spectralon sample holders of 10 mm diameter. Quantum yields were determined using a

sample of finely powdered $BaSO_4$ as a non-emissive blank. Scattered light at λ_{ex} = 425 nm for sample and blank was measured using a neutral density filter of O.D. = 2, whilst the emission region was monitored in the absence of the filter. A Synapse CCD detector was used for detection of the emitted light, which offers better sensitivity in the red / NIR region compared to the R928 PMT. Luminescence lifetimes at ambient temperature were measured by time-correlated single-photon counting (TCSPC) following excitation using a pulsed laser diode at 405 nm and using an R928 PMT for detection. The same detector operating in multi-channel scaling (MCS) mode was used to measure the longer lifetimes at 77 K, following excitation with a pulsed xenon flashlamp.

Theoretical Calculations

All calculations were done in the gas phase with the Gaussian 09 (Revision B.01) software package[52] employing B3LYP[53-55] (for DFT) and long-range corrected CAM-B3LYP[56] (for TD-DFT) functionals (Figures S45-47). Similar complexes containing Cu_2X_2 cores supported by *P^N* ligands were found to have strong CT character, in particular (Cu+X)LCT,[18, 21, 39] and so, range-separated hybrids were employed for CT-type transitions to ensure physically meaningful estimates of the transition energies.[40] Basis sets 6-31G(d,p)[57-58] on H, C, N and P; m6-31G(d) [59] on Cu; and LANL2DZ with effective core potential[60-62] on I were employed for all calculations. The effect of zero-point energy of molecular vibrations was not considered in this study. Molecular orbital analyses were carried out with QMForge[56] and visualized with Avogadro,[63] while TD-DFT results were analyzed using GaussSum software package (FWHM: 3000 cm^{-1}, σ = 0.2).[64]

To calculate ground-state, excited-state and reorganization energies,[43] the following protocol was followed using the method described above for both **2-I** and **3-I**: (1) The S_0 geometry was optimized by restricted DFT (charge = 0, multiplicity = 1) using the crystal structure coordinates as starting input. The T_1 geometry was optimized with unrestricted DFT (charge = 0, multiplicity = 3) using the optimized S_0 geometry as starting input. Frequency calculations were then subsequently carried out to confirm that these structures are at a minimum and to derive free energies. (2) To determine the relative atomic contributions to the frontier MOs of **2-I** and **3-I**, Mulliken population analyses (keyword: Pop=full) were carried out on the optimized structures of S_0 and T_1. Another population analysis was carried out on S_0 using the optimized T_1 coordinates (T_1@S_0). The electronic energies, $E(S_0)$ and $E(T_1)$, obtained from the single point calculations of S_0 and T_1 in their respective minimum were used to estimate the adiabatic energy (E^{adia}), where, $E^{adia} = E(T_1) - E(S_0)$. (3) TD-DFT was then carried out on the following: (a) $S_n \leftarrow S_0$ singlet-singlet transitions (first 20 transitions for **3-I**; first 10 transitions for **2-I**) with the restricted formalism with charge = 0 and multiplicity = 1; (b) $T_n \leftarrow (T_1@S_0)$ singlet-triplet transitions (first 10 transitions for both **2-I** and **3-I**) with the unrestricted formalism, but keeping the same charge and multiplicity as in (a). These gave $E^{vert\text{-}abs}$ and $E^{vert\text{-}phos}$ as shown in Figure S48. The reorganization energy (λ_T) after the emission of light was then calculated as $\lambda_T = E^{adia} - E^{vert\text{-}phos}$.

ASSOCIATED CONTENT

Supporting Information. Multi-nuclear NMR spectra of all new compounds; additional UV-Vis absorption and emission spectra; details of computational methods; combined crystallographic information file containing all X-ray data. CCDC 1811419-1811424 contain the supplementary crystallographic data for this paper. The data can be obtained free of charge from The Cambridge Crystallographic Data Centre via www.ccdc.cam.ac.uk/structures.

The following files are available free of charge:

Supporting Information File (PDF)

Combined Crystallographic Information File (CIF)

AUTHOR INFORMATION

Corresponding Authors

*david.herbert@umanitoba.ca

*j.a.g.williams@durham.ac.uk

ORCID

Rebecca L. Davis: 0000-0002-0679-6025

David E. Herbert: 0000-0001-8190-2468

J. A. Gareth Williams: 0000-0002-4688-3000

Author Contributions

The manuscript was written through contributions of all authors. All authors have given approval to the final version of the manuscript.

Funding Sources

The following sources are gratefully acknowledged: Natural Sciences Engineering Research Council of Canada for a Discovery Grant to DEH (RGPIN-2014-03733); the Canadian Foundation for Innovation and Research Manitoba for an award in support of an X-ray diffractometer (CFI #32146); the University of Manitoba for start-up funding (DEH) and GETS support (RM, IBML). The Association of Commonwealth Universities (ACU) is thanked for a University of Manitoba Titular Fellowship (2016–17) to JAGW.

ACKNOWLEDGMENTS

We are grateful to Prof. Mazdak Khajehpour for access to a UV-Vis spectrometer and Prof. Viktor N. Nemykin for helpful discussions.

REFERENCES

1. Li, Z.; Sun, W. Synthesis, Photophysics, and Reverse Saturable Absorption of Platinum Complexes Bearing Extended π-Conjugated CNN Ligands. *Dalton Trans.* **2013**, *42*, 14021-14029.

2. Sicilia, V.; Fuertes, S.; Martin, A.; Palacios, A. N-Assisted CPh-H Activation in 3,8-Dinitro-6-phenylphenanthridine. New C,N-Cyclometalated Compounds of Platinum(II): Synthesis, Structure, and Luminescence Studies. *Organometallics* **2013**, *32*, 4092-4102.

3. Li, Z.; Cui, P.; Wang, C.; Kilina, S.; Sun, W. Nonlinear Absorbing Cationic Bipyridyl Iridium(III) Complexes Bearing Cyclometalating Ligands with Different Degrees of π-Conjugation: Synthesis, Photophysics, and Reverse Saturable Absorption. *J. Phys. Chem. C* **2014**, *118*, 28764-28775.

4. Jiang, B.; Gu, Y.; Qin, J.; Ning, X.; Gong, S.; Xie, G.; Yang, C. Deep-Red Iridium(III) Complexes Cyclometalated by Phenanthridine Derivatives for Highly Efficient Solution-Processed Organic Light-Emitting Diodes. *J. Mat. Chem. C* **2016**, *4*, 3492-3498.

5. Bossi, A.; Rausch, A. F.; Leitl, M. J.; Czerwieniec, R.; Whited, M. T.; Djurovich, P. I.; Yersin, H.; Thompson, M. E. Photophysical Properties of Cyclometalated Pt(II) Complexes: Counterintuitive Blue Shift in Emission with an Expanded Ligand π System. *Inorg. Chem.* **2013**, *52*, 12403-12415.

6. Liu, B.; Lystrom, L.; Kilina, S.; Sun, W. Tuning the Ground State and Excited State Properties of Monocationic Iridium(III) Complexes by Varying the Site of Benzannulation on Diimine Ligand. *Inorg. Chem.* **2017**, *56*, 5361-5370.

7. Hanson, K.; Roskop, L.; Djurovich, P. I.; Zahariev, F.; Gordon, M. S.; Thompson, M. E. A Paradigm for Blue- or Red-Shifted Absorption of Small Molecules Depending on the Site of π-Extension. *J. Am. Chem. Soc.* **2010**, *132*, 16247-16255.

8. Mondal, R.; Giesbrecht, P. K.; Herbert, D. E. Nickel(II), Copper(I) and Zinc(II) Complexes Supported by a (4-Diphenylphosphino)phenanthridine Ligand. *Polyhedron* **2016**, *108*, 156-162.

9. Mandapati, P.; Giesbrecht, P. K.; Davis, R. L.; Herbert, D. E. Phenanthridine-Containing Pincer-like Amido Complexes of Nickel, Palladium, and Platinum. *Inorg. Chem.* **2017**, *56*, 3674-3685.

10. Ford, P. C.; Cariati, E.; Bourassa, J. Photoluminescence Properties of Multinuclear Copper(I) Compounds. *Chem. Rev.* **1999**, *99*, 3625-3648.

11. Armaroli, N.; Accorsi, G.; Cardinali, F.; Listorti, A., Photochemistry and Photophysics of Coordination Compounds: Copper. In *Photochemistry and Photophysics of Coordination Compounds I*, Balzani, V.; Campagna, S., Eds. Springer-Verlag Berlin: Berlin, **2007**; Vol. 280, pp 69-115.

12. Peng, R.; Li, M.; Li, D. Copper(I) Halides: A Versatile Family in Coordination Chemistry and Crystal Engineering. *Coord. Chem. Rev.* **2010**, *254*, 1-18.

13. Tsuge, K.; Chishina, Y.; Hashiguchi, H.; Sasaki, Y.; Kato, M.; Ishizaka, S.; Kitamura, N. Luminescent Copper(I) Complexes With Halogenido-Bridged Dimeric Core. *Coord. Chem. Rev.* **2016**, *306*, 636-651.

14. Cariati, E.; Lucenti, E.; Botta, C.; Giovanella, U.; Marinotto, D.; Righetto, S. Cu(I) Hybrid Inorganic-Organic Materials With Intriguing Stimuli Responsive and Optoelectronic Properties. *Coord. Chem. Rev*. **2016**, *306*, 566-614.

15. Yersin, H.; Rausch, A. F.; Czerwieniec, R.; Hofbeck, T.; Fischer, T. The Triplet State of Organo-Transition Metal Compounds. Triplet Harvesting and Singlet Harvesting for Efficient OLEDs. *Coord. Chem. Rev*. **2011**, *255*, 2622-2652.

16. Czerwieniec, R.; Leitl, M. J.; Homeier, H. H. H.; Yersin, H. Cu(I) Complexes - Thermally Activated Delayed Fluorescence. Photophysical Approach and Material Design. *Coord. Chem. Rev*. **2016**, *325*, 2-28.

17. Maksić, Z. B.; Barić, D.; Müller, T. Clar's Sextet Rule Is a Consequence of the σ-Electron Framework. *J. Phys. Chem. A* **2006**, *110*, 10135-10147.

18. Zeng, C.; Wang, N.; Peng, T.; Wang, S. Copper(I) Complexes Bearing 1,2-Phenyl-Bridged P^N, P^N^P, and N^P^N Chelate Ligands: Structures and Phosphorescence. *Inorg. Chem*. **2017**, *56*, 1616-1625.

19. Macrae, C. F.; Bruno, I. J.; Chisholm, J. A.; Edgington, P. R.; McCabe, P.; Pidcock, E.; Rodriguez-Monge, L.; Taylor, R.; van de Streek, J.; Wood, P. A. Mercury CSD 2.0 - New Features for the Visualization and Investigation of Crystal Structures. *J. Appl. Cryst*. **2008**, *41*, 466-470.

20. Montalti, M.; Credi, A.; Prodi, L.; Gandolfi, M., *Handbook of Photochemistry*. 3rd ed.; CRC Press: Boca Raton, **2006**; p 664.

21. Leitl, M. J.; Kuechle, F.-R.; Mayer, H. A.; Wesemann, L.; Yersin, H. Brightly Blue and Green Emitting Cu(I) Dimers for Singlet Harvesting in OLEDs. *J. Phys. Chem. A* **2013**, *117*, 11823-11836.

22. Araki, H.; Tsuge, K.; Sasaki, Y.; Ishizaka, S.; Kitamura, N. Luminescence Ranging from Red to Blue: A Series of Copper(I)−Halide Complexes Having Rhombic {Cu2(μ-X)2} (X = Br and I) Units with N-Heteroaromatic Ligands. *Inorg. Chem.* **2005**, *44*, 9667-9675.

23. Zink, D. M.; Baechle, M.; Baumann, T.; Nieger, M.; Kuehn, M.; Wang, C.; Klopper, W.; Monkowius, U.; Hofbeck, T.; Yersin, H.; Brase, S. Synthesis, Structure, and Characterization of Dinuclear Copper(I) Halide Complexes with P^N Ligands Featuring Exciting Photoluminescence Properties. *Inorg. Chem.* **2013**, *52*, 2292-2305.

24. Englman, R.; Jortner, J. The Energy Gap Law for Radiationless Transitions in Large Molecules. *Mol. Phys.* **1970**, *18*, 145-164.

25. Caspar, J. V.; Kober, E. M.; Sullivan, B. P.; Meyer, T. J. Application of the Energy Gap Law to the Decay of Charge-Transfer Excited States. *J. Am. Chem. Soc.* **1982**, *104*, 630-632.

26. Caspar, J. V.; Meyer, T. J. Application of the Energy Gap Law to Nonradiative, Excited-State Decay. *J. Phys. Chem.* **1983**, *87*, 952-7.

27. Kober, E. M.; Caspar, J. V.; Lumpkin, R. S.; Meyer, T. J. Application of the Energy Gap Law to Excited-State Decay of Osmium(II)-Polypyridine Complexes:

Calculation of Relative Nonradiative Decay Rates from Emission Spectral Profiles. *J. Phys. Chem.* **1986**, *90*, 3722-34.

28. Whittle, C. E.; Weinstein, J. A.; George, M. W.; Schanze, K. S. Photophysics of Diimine Platinum(II) Bis-Acetylide Complexes. *Inorg. Chem.* **2001**, *40*, 4053-4062.

29. Wilson, J. S.; Chawdhury, N.; Al-Mandhary, M. R. A.; Younus, M.; Khan, M. S.; Raithby, P. R.; Koehler, A.; Friend, R. H. The Energy Gap Law for Triplet States in Pt-Containing Conjugated Polymers and Monomers. *J. Am. Chem. Soc.* **2001**, *123*, 9412-9417.

30. Nitsch, J.; Lacemon, F.; Lorbach, A.; Eichhorn, A.; Cisnetti, F.; Steffen, A. Cuprophilic Interactions in Highly Luminescent Dicopper(I)-NHC-Picolyl Complexes - Fast Phosphorescence or TADF? *Chem. Commun.* **2016**, *52*, 2932-2935.

31. Zander, M. The Significance of Donor-Acceptor Interactions in the External Heavy Atom Effect of Silver Nitrate on the Luminescence Behavior of Aza-Aromatic Systems and Carbazoles. *Z. Naturforsch., A* **1978**, *33A*, 998-1000.

32. Najbar, J.; Jarzeba, W.; Urbanek, Z. H. Internal Heavy-Atom Effect on the T1 States of Monochloroquinolines and Monochloronaphthalenes. *Chem. Phys.* **1983**, *79*, 245-53.

33. de Groot, M. S.; van der Waals, J. H. Paramagnetic Resonance in Phosphorescent Aromatic Hydrocarbons. III. Conformational Isomerism in Benzene and Triptycene. *Mol. Phys.* **1963**, *6*, 545-62.

34. de Groot, M. S.; Hesselmann, I. A. M.; van der Waals, J. H. Electron Resonance of Phosphorescent Mesitylene. *Mol. Phys.* **1965**, *10*, 91-3.

35. Rabalais, J. W.; Maria, H. J.; McGlynn, S. P. Phosphorescence Decay of Benzene and Methylbenzene Derivatives. *J. Chem. Phys.* **1969**, *51*, 2259-73.

36. Buma, W. J.; Van der Waals, J. H.; Van Hemert, M. C. Conformational Instability of the Lowest Triplet State of Benzene: the Result of Ab Initio Calculations. *J. Am. Chem. Soc.* **1989**, *111*, 86-7.

37. Summerville, R. H.; Hoffmann, R. Tetrahedral and Other M2L6 Transition Metal Dimers. *J. Am. Chem. Soc.* **1976**, *98*, 7240-54.

38. Aullon, G.; Ujaque, G.; Lledos, A.; Alvarez, S.; Alemany, P. To Bend or Not To Bend: Dilemma of the Edge-Sharing Binuclear Square Planar Complexes of d8 Transition Metal Ions. *Inorg. Chem.* **1998**, *37*, 804-813.

39. Wei, F.; Liu, X.; Liu, Z.; Bian, Z.; Zhao, Y.; Huang, C. Structural and Photophysical Study of Copper Iodide Complex with P^N or P^N^P Ligand. *CrystEngComm* **2014**, *16*, 5338-5344.

40. Adamo, C.; Jacquemin, D. The calculations of excited-state properties with Time-Dependent Density Functional Theory. *Chem. Soc. Rev.* **2013**, *42*, 845-856.

41. Yang, L.; Powell, D. R.; Houser, R. P. Structural Variation in Copper(I) Complexes with Pyridylmethylamide Ligands: Structural Analysis With a New Four-Coordinate Geometry Index, $\tau 4$. *Dalton Trans.* **2007**, 955-964.

42. Cunningham, C. T.; Moore, J. J.; Cunningham, K. L. H.; Fanwick, P. E.; McMillin, D. R. Structural and Photophysical Studies of Cu(NN)2+ Systems in the Solid State. Emission at Last from Complexes with Simple 1,10-Phenanthroline Ligands. *Inorg. Chem*. **2000**, *39*, 3638-3644.

43. Uoyama, H.; Goushi, K.; Shizu, K.; Nomura, H.; Adachi, C. Highly Efficient Organic Light-Emitting Diodes From Delayed Fluorescence. *Nature* **2012**, *492*, 234-238.

44. Hamze, R.; Jazzar, R.; Soleilhavoup, M.; Djurovich, P. I.; Bertrand, G.; Thompson, M. E. Phosphorescent 2-, 3- and 4-Coordinate Cyclic (Alkyl)(amino)carbene (CAAC) Cu(I) Complexes. *Chem. Commun.* **2017**, *53*, 9008-9011.

45. He, L.-H.; Luo, Y.-S.; Di, B.-S.; Chen, J.-L.; Ho, C.-L.; Wen, H.-R.; Liu, S.-J.; Wang, J.-Y.; Wong, W.-Y. Luminescent Three- and Four-Coordinate Dinuclear Copper(I) Complexes Triply Bridged by Bis(diphenylphosphino)methane and Functionalized 3-(2′-Pyridyl)-1,2,4-triazole Ligands. *Inorg. Chem*. **2017**, *56*, 10311-10324.

46. Hupp, B.; Schiller, C.; Lenczyk, C.; Stanoppi, M.; Edkins, K.; Lorbach, A.; Steffen, A. Synthesis, Structures, and Photophysical Properties of a Series of Rare Near-IR Emitting Copper(I) Complexes. *Inorg. Chem*. **2017**, *56*, 8996-9008.

47. Kim, Y.-E.; Kim, J.; Park, J. W.; Park, K.; Lee, Y. [σ]-Complexation as a Strategy for Designing Copper-based Light Emitters. *Chem. Commun.* **2017**, *53*, 2858-2861.

48. Lee, C.-I.; Zhou, J.; Ozerov, O. V. Catalytic Dehydrogenative Borylation of Terminal Alkynes by a SiNN Pincer Complex of Iridium. *J. Am. Chem. Soc.* **2013**, *135*, 3560-3566.

49. Bruker-AXS *APEX3 v2016.1-0*, Madison, Wisconsin, USA, **2016**.

50. Sheldrick, G. M. A Short History of SHELX. *Acta Cryst.* **2008**, *A64*, 112-122.

51. Spek, A. L. Structure Validation in Chemical Crystallography. *Acta Cryst.* **2009**, *D65*, 148-155.

52. Frisch, M. J. T., G. W.; Schlegel, H. B.; Scuseria, G. E.; Robb, M. A.; Cheeseman, J. R.;; Scalmani, G. B., V.; Mennucci, B.; Petersson, G. A.; Nakatsuji, H.; Caricato, M.; Li, X.;; Hratchian, H. P. I., A. F.; Bloino, J.; Zheng, G.; Sonnenberg, J. L.; Hada, M.; Ehara, M.;; Toyota, K. F., R.; Hasegawa, J.; Ishida, M.; Nakajima, T.; Honda, Y.; Kitao, O.; Nakai, H.;; Vreven, T. M., Jr., J. A.; Peralta, J. E.; Ogliaro, F.; Bearpark, M.; Heyd, J. J.; Brothers,; E.; Kudin, K. N. S., V. N.; Kobayashi, R.; Normand, J.; Raghavachari, K.; Rendell, A.;; Burant, J. C. I., S. S.; Tomasi, J.; Cossi, M.; Rega, N.; Millam, J. M.; Klene, M.; Knox, J.; E.; Cross, J. B. B., V.; Adamo, C.; Jaramillo, J.; Gomperts, R.; Stratmann, R. E.; Yazyev,; O.; Austin, A. J. C., R.; Pomelli, C.; Ochterski, J. W.; Martin, R. L.; Morokuma, K.;; Zakrzewski, V. G. V., G. A.; Salvador, P.; Dannenberg, J. J.; Dapprich, S.; Daniels, A. D.;; Farkas, Ö. F., J. B.; Ortiz, J. V.; Cioslowski, J.; Fox, D. J. *Gaussian 09 Program Package, Revision B.01*, Gaussian, Inc.: Wallingford, CT, **2009**.

53. Lee, C.; Yang, W.; Parr, R. G. Development of the Colle-Salvetti Correlation-Energy Formula into a Functional of the Electron Density. *Phys. Rev. B: Condens. Matter* **1988**, *37*, 785-9.

54. Becke, A. D. A New Mixing of Hartree-Fock and Local-Density-Functional Theories. *J. Chem. Phys.* **1993**, *98*, 1372-7.

55. Becke, A. D. Density-Functional Thermochemistry. III. The Role of Exact Exchange. *J. Chem. Phys.* **1993**, *98*, 5648-52.

56. Yanai, T.; Tew, D. P.; Handy, N. C. A New Hybrid Exchange-Correlation Functional Using the Coulomb-Attenuating Method (CAM-B3LYP). *Chem. Phys. Lett.* **2004**, *393*, 51-57.

57. Hariharan, P. C.; Pople, J. A. Influence of Polarization Functions on MO Hydrogenation Energies. *Theor. Chim. Acta* **1973**, *28*, 213-22.

58. Francl, M. M.; Pietro, W. J.; Hehre, W. J.; Binkley, J. S.; Gordon, M. S.; DeFrees, D. J.; Pople, J. A. Self-Consistent Molecular Orbital Methods. XXIII. A Polarization-Type Basis Set for Second-Row Elements. *J. Chem. Phys.* **1982**, *77*, 3654-65.

59. Mitin, A. V.; Baker, J.; Pulay, P. An Improved 6-31G* Basis Set for First-Row Transition Metals. *J. Chem. Phys.* **2003**, *118*, 7775-7782.

60. Hay, P. J.; Wadt, W. R. Ab Initio Effective Core Potentials for Molecular Calculations. Potentials for Potassium to Gold Including the Outermost Core Orbitals. *J. Chem. Phys.* **1985**, *82*, 299-310.

61. Hay, P. J.; Wadt, W. R. Ab Initio Effective Core Potentials for Molecular Calculations. Potentials for the Transition Metal Atoms Scandium to Mercury. *J. Chem. Phys.* **1985**, *82*, 270-83.

62. Wadt, W. R.; Hay, P. J. Ab Initio Effective Core Potentials for Molecular Calculations. Potentials for Main Group Elements Sodium to Bismuth. *J. Chem. Phys.* **1985**, *82*, 284-298.

63. Hanwell, M. D.; Curtis, D. E.; Lonie, D. C.; Vandermeersch, T.; Zurek, E.; Hutchison, G. R. Avogadro: an Advanced Semantic Chemical Editor, Visualization, and Analysis Platform. *J. Cheminf.* **2012**, *4*, 17.

64. O'Boyle, N. M.; Tenderholt, A. L.; Langner, K. M. Software News and Updates cclib: a Library for Package-Independent Computational Chemistry Algorithms. *J. Comput. Chem.* **2008**, *29*, 839-845.

FOR TABLE OF CONTENTS ONLY

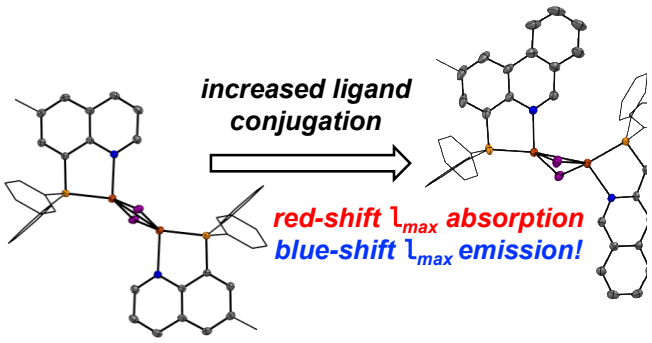

SYNOPSIS

Orange-red phosphorescent, halide-bridged $[(P\text{^}N)Cu(I)]_2(\mu\text{-}X)_2$ dimers with benzannulated pyridine ligands show a counter-intuitive dependence of emission maxima on π-extension, where contrary to conventional assumptions and a bathochromic shift in the lowest energy absorption maxima, a blue shift of nearly 40 nm in the emission wavelength is observed for complexes with larger, more rigid ligand π-systems.